Crystallographic texture in Materials

Satyam Suwas AND Nilesh P. Gurao

Abstract | Many naturally occurring as well as man made materials comprise of large number of crystallites with a preferred orientation. The preferred orientation, popularly known as texture, governs various structural and mechanical properties of these materials. Texture may develop during variety of processes like solidification, plastic deformation, annealing and phase transformation. It is, therefore, possible to tailor texture in materials to enhance a particular property. Traditionally, X-ray and neutron diffraction had been used to study texture in materials. It has been very recently that other techniques based on synchrotron X-rays and SEM based Electron Backscattered Diffraction have been developed for complete characterization of texture in materials. In the present review, the authors discuss the pole figures and more comprehensive orientation distribution function methods for texture analysis. In addition, a brief account of texture evolution in various technologically important materials, ranging from common metals and alloys to intermetallics, ceramics and polymers along with some naturally occurring materials like rocks, ice, bones etc. has been given. The present review is particularly aimed at readers newly initiated in this field rather than the experts.

1. Introduction

It has been known since long time that microstructure plays an important role in deciding the properties of materials. Most of the engineering materials are polycrystalline in nature excluding a few ones. In such a case, microstructure can be considered as the combination of morphology and orientation of the constituents. The former refers to shape of the constituents, while the latter is connected with its crystallography. Therefore, texture is a constituent feature of microstructure. In German language, the word '*gefuge*' includes both microstructure and texture.

Texture is derived from the latin word 'textor' meaning weaver. In materials science, texture refers to how a material is woven. In the simplest words, one can define texture as the arrangement of building blocks in the polycrystalline material [1]. Figs. 2(a and b) show a sheet of polycrystalline material depicting two situations (a) where the constituent grains are crystallographically

similarly arranged, (b) the constituent grains are crystallographically differently arranged. The first situation will lead to a single crystal while the second would lead to a random polycrystal. There could be a third situation as well, where some of the grains are similarly arranged, while the others are differently arranged (Fig. 2c). A powder photograph from the three materials is shown in Fig. 3.

The aim of materials scientists engaged in texture research is to develop materials with favourable properties. The properties of polycrystalline materials depend on the individual properties of the single crystals and also on parameters characterizing the polycrystalline state. When all possible orientations of the crystallites occur with equal frequency, the orientation dependence of properties will disappear due to averaging, and the polycrystalline material can be said isotropic. However, complete isotropic characteristics are difficult to achieve and many a times not desirable. A typical instance is the sheet metals used for

Department of Materials Engineering, Indian Institute of Science, Bangalore 560012, India
satyamsuwas@materials.iisc.ernet.in

Dedication: **Dedicated to Professor Ranjit Kumar Ray, for his immense contribution to this subject**

Figure 1: Unique grain colour map of titanium in EBSD wherein individual grain is represented by a separate colour with the orientation of the lattice superimposed on it.

crystals are nearly similarly oriented, the behaviour of the polycrystalline material in many respects is close to that of a single crystal. A prominent example of this case is the so-called "cube texture" in face centre or body centre cubic materials. In that case, all grains are oriented so that the {0 0 1} planes lie nearly parallel to the plane of the sheet and the <100> directions point approximately in the rolling direction. The texture {0 0 1} <100> is highly desirable in substrates for high T_c superconductors. This texture as well as another texture known as Goss texture {1 1 0} <001> are usually desired in magnetic materials, in which it is easy to magnetize in the cube edge <100> direction (Fig. 5). There are several other examples, where a particular texture is desirable or undesirable. The list could be quite exhaustive and therefore, not possible to present in this review.

It is well established that crystallographic texture is an inherent characteristic of metals, ceramics, polymers and geological materials and has a significant influence on mechanical, physical as well as chemical properties of materials. Some properties where the role of texture is well established are strength, ductility modules of elasticity, electrical conductivity, piezoelectricity, magnetic susceptibility, light refraction and wave propagation. In the past century, most of the studies

deep drawing; the semi-isotropic characteristic is required in order to avoid undesirable ears (Fig. 4b). This requires a complicated treatment of the sheet material. On the other hand, if all

Figure 2: Schematic representation of sheet of polycrystalline material with constituent grains (a) arranged in a crystallographically similar way (b) in a crystallographically different way (c) some grains crystallographically arranged in a similar way while others are randomly arranged.
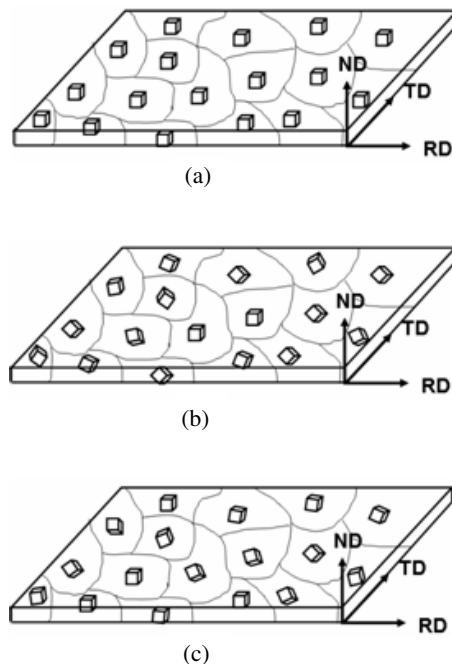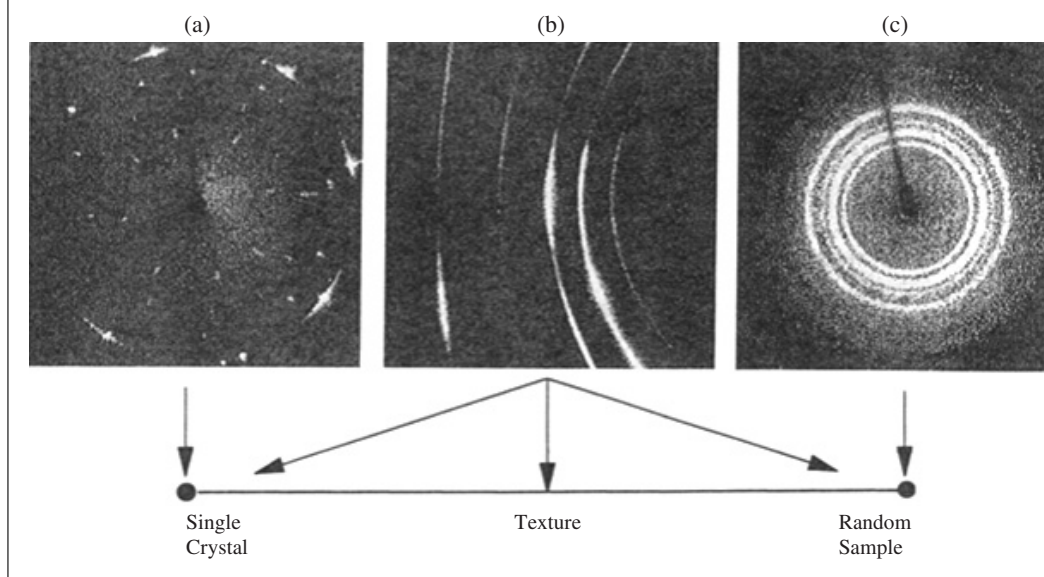

(a)

(b)

(c)

Figure 3: X-ray powder photograph from the materials mentioned in Fig. 2. [22].

(a)   (b)   (c)

Single Crystal   Texture   Random Sample

on texture have been carried out on metals and alloys; however, recently it has gained importance in structural and functional ceramics (e.g. high temperature superconductors) as well as polymers. Moreover, new applications of texture control have emerged in thin films, coatings and electronic instruments.

2. Representation of texture

The texture in rolled sheet material, is commonly represented by {hkl} [uvw], which means the {hkl} planes of these grains lie parallel to the sheet plane, whereas their [uvw] direction point parallel to the rolling direction [3–4]. For material with only one important dimension like extruded rods, wires,

Figure 4: Aluminium cup (a) without ears, (b) with ears (courtesy Vaw Aluminium AG, Bonn).

(a)   (b)

thin films or any one of these two sets are used to describe texture. When the texture is less complex, it is possible to describe the texture by one or a series of pole figures determined by simple X-ray diffraction methods. The information contained in a pole figures is however, incomplete and at best semi-quantitative. In fact, it is frequently not sufficient to fully determine the true and complete texture if the crystallites possess more than one preferred (ideal) orientation. The more complete representation is by orientation distribution function [5–6]. However, these are not directly measured by simple X-ray diffraction, and need further derivations and calculations based on a number of experimentally measured pole figures.

### 2.1. *Texture description by means of pole figures*

The pole figure is the two-dimensional stereographic projection, with crystal orientation specified relative to the specimen geometry, which shows the variation of pole density with pole orientation for a selected set of crystal plane {hkl}. They are rather the disposition of plane normals. The most popular way to obtain the incomplete pole figure is the "Schultz reflection method" [7].

Detailed descriptions of the X-ray methods that lead to the determination of pole figures can be found in the monograph "Textures in metals" due to Heatherly and Hutchinson [1]; in a comprehensive article by Cahn [8] in his famous series on Materials Science and Technology; in the book by Kocks, Tome and Wenk [9] and in other texts on X-ray diffraction [3–4]. From the inspection of a

Figure 5: (a) Magnetic anisotropy in rolled Fe–Si alloy from [1] (b) Schematic arrangement of the unit cells in the rolled sheet of Fe–Si alloy with a strong Goss {110}<001> and Cube {001}<100> component.
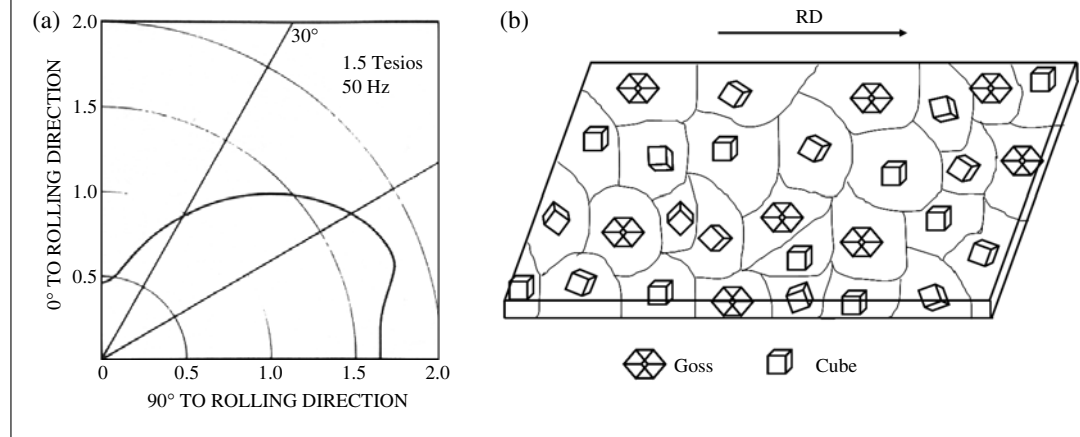
pole figure data, it is possible to describe a well developed texture by relating the positions and intensities of specific orientations with those of the specimen geometry. For example, textures in rolled sheet metals are frequently represented as being of the type {hkl} <uvw>, which means that the orientations of the grains in the sheet are such that their {hkl} planes lie parallel to the plane of the sheet (i.e. perpendicular to the normal direction (ND)), whereas their <uvw> directions lie parallel to the rolling direction (RD). When the texture is more complex, as usually the case, it is possible to describe it as consisting of a number of components of different severity such as

Overall texture = $\sum \lambda_i \cdot \{hkl\}_i <uvw>_i$

Here, λ_i is a weighting factor which is introduced to allow for the relative intensities or strengths of the various components.

The positions of the (111) and (200) poles of some useful texture components are presented in Fig. 6(a and b). The famous copper {112} <111>, brass {110} <112> and S {123} <634> orientations, which are the major components of the deformation texture in FCC materials, are shown in Fig. 6a. The cube, {100} <001>, which is the major component of the recrystallisation texture in FCC materials and is technically very important, is also displayed in this pole figure. The (200) poles of the main components of the BCC transformation textures in steels are illustrated in Fig. 6b. Of these, the {332} <113> component forms by transformation from the {110} <112> orientation present in the deformed austenite (Fig. 6a), and the {113} <110> component is derived in a similar way from the FCC {112} <111> orientation. Furthermore, the {100} <001> BCC component

is also the major recrystallisation component in FCC austenite. Therefore, by recording the relevant pole figure at different stages of processing, one can correlate with the physical phenomenon during phase transformation. Fig. 6c shows the experimentally measured pole (111) and (200) pole figures for a FCC (copper) and BCC (Low cost β Titanium alloy) material respectively.

2.2. Texture description by means of orientation distribution functions

Although pole figures provide a useful description of the texture present in a material, the information they contain is incomplete and at best semi-quantitative. This difficulty can be removed by the use of the crystallite orientation distribution function (CODF or ODF), which describes the frequency of occurrence of particular orientations in a three-dimensional orientation space. This space is defined by three Euler angles which constitute a set of three consecutive rotations that must be given to each crystallite in order to bring its crystallographic axes into coincidence with the specimen axes. The complete ODF consists of the sets of rotations pertaining to all the crystallites in the specimen. Mathematical models have been developed which allow the ODF to be calculated from the numerical data obtained from several pole figures.

The most widely adopted methods are those proposed independently by Roe [5] and by Bunge [6], who used generalized spherical harmonic functions to represent the crystallite distributions. A thorough mathematical treatment of this subject can be found in book Bunge [10]. The three Euler angles employed by Bunge to describe the crystal rotations are ϕ_1, ϕ, and ϕ_2, whereas the set of angles

Figure 6: Important texture components (a) in (111) pole figure for rolled austenite (b) in (200) pole figure for ferrite (c) experimentally measured (111) and (200) pole figures of rolled copper and Low cost beta Titanium alloy respectively.
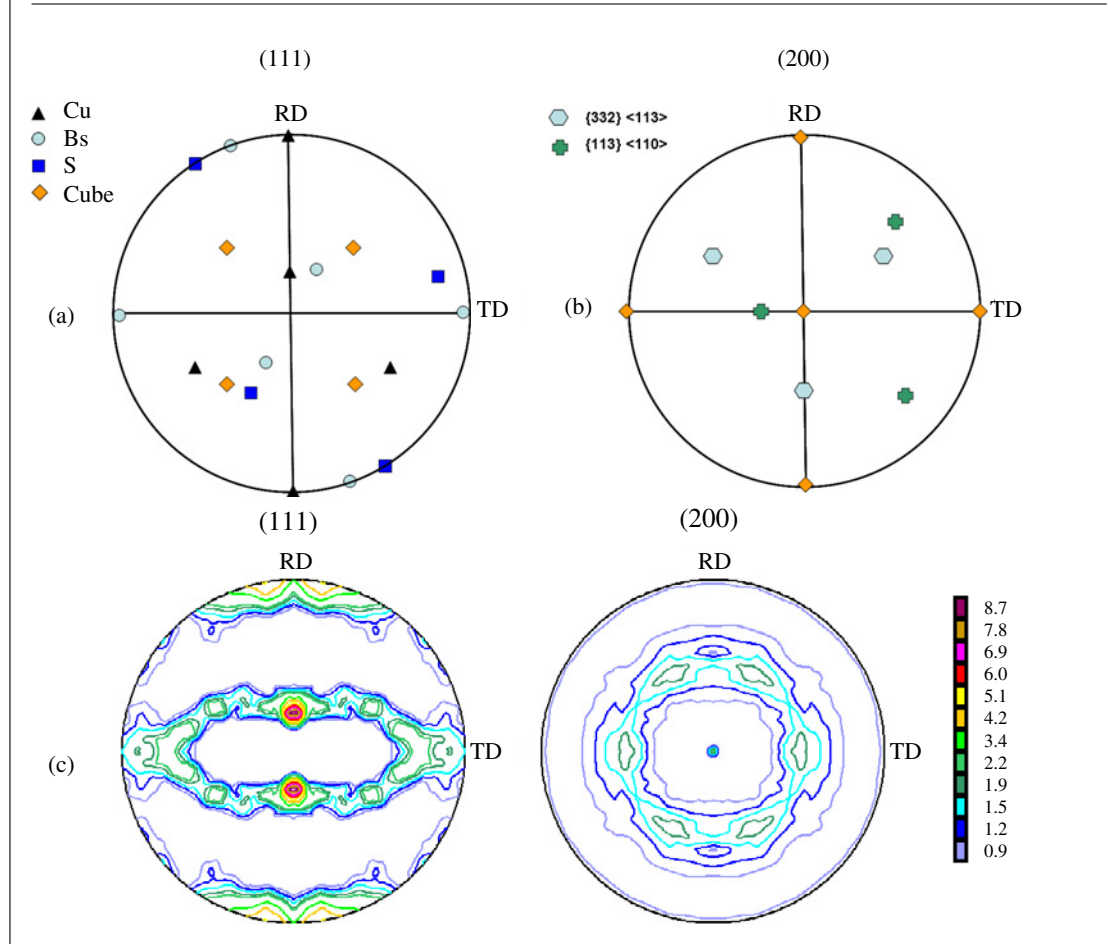
proposed by Roe are referred to as Ψ, Θ, and Φ, respectively.

According to Bunge, an ODF may be expressed as a series of generalized spherical harmonics in the form:

$$f(\phi_1, \phi, \phi_2) = \sum_{1=0}^{\infty} \sum_{m=-1}^{+1} \sum_{n=-1}^{+1} C_1^{mn} P_1^{mn}(\phi)$$
$$\times \exp(im\phi_2) \exp(in\phi_1)$$

where C_1^{mn} are the series coefficients and $P_1^{mn}(\phi)$ are certain generalizations of the associated Legendre functions.

In Roe's notation, an ODF may be expressed as

$$\omega(\Psi, \Theta, \Phi) = \sum_{1=0}^{\infty} \sum_{m=-1}^{+1} \sum_{n=-1}^{+1} W_{1mn} Z_{1mn}(\cos\theta)$$
$$\times \exp(-im\psi) \exp(in\phi)$$

where, W_{1mn} are the series coefficients and Z_{1mn} ($\cos \theta$) is a generalization of the associated

Legendre functions, the so called augmented Jacobi polynomials. The relationships between the Roe and Bunge angles are the following

$$\phi_1 = \frac{\pi}{2} - \Psi; \phi = \Theta; \phi_2 = \frac{\pi}{2} - \Phi$$

For cubic/orthorhombic crystal/specimen symmetry, a three-dimensional orientation volume may be defined by using three orthogonal axes for ϕ_1, ϕ and ϕ_2 with each of the Euler angles ranging from 0 to 90° [11]. This volume is divided into three basic ranges in which each orientation appears once. The value of the orientation density at each point in this volume is simply the strength or intensity of that orientation in multiplies of random units. Regions of higher and lower orientation density are separated by three dimensional contour surfaces and it is usual to take a series of parallel sections through this space for ready two dimensional visualization of the data contained in the three dimensional plot. It is to be mentioned here that the spherical harmonic

Figure 7: (a) The three Euler angles (b) 3D view of Euler Space (c) $\Phi = 45°$ section (Bunge notation) and (d) $\Phi = 45°$ (Roe notation) in Euler space [54].
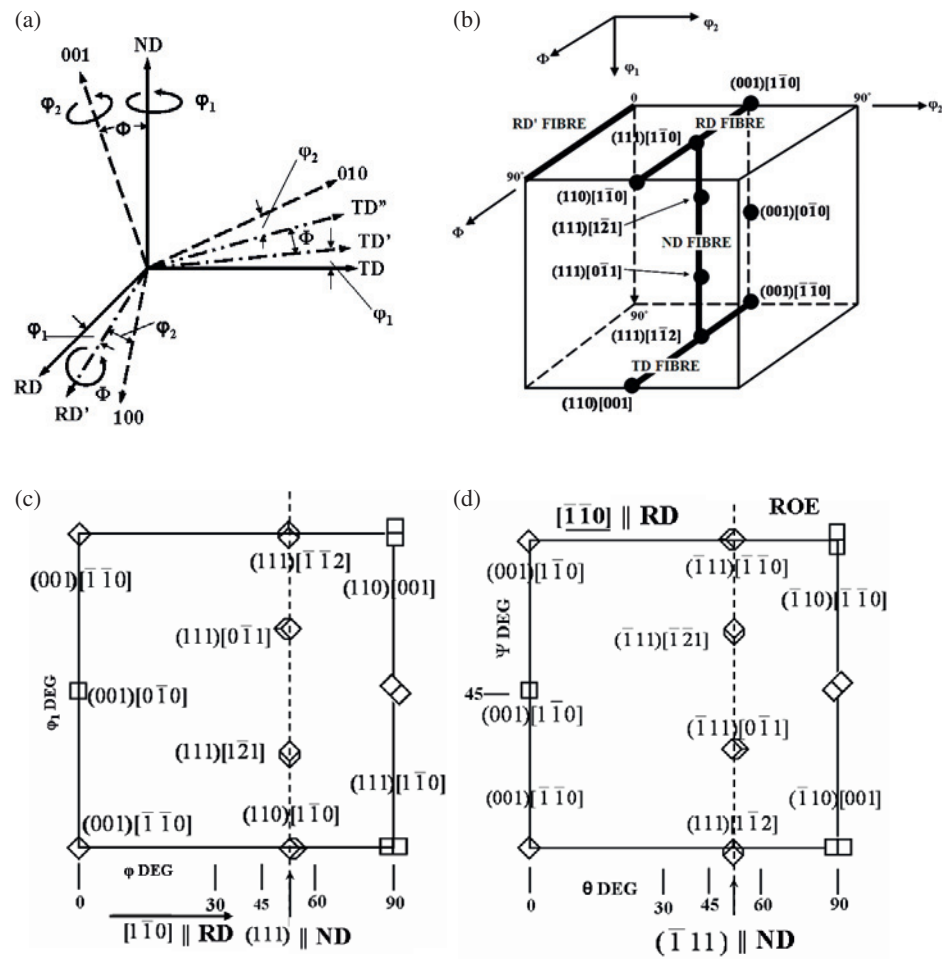

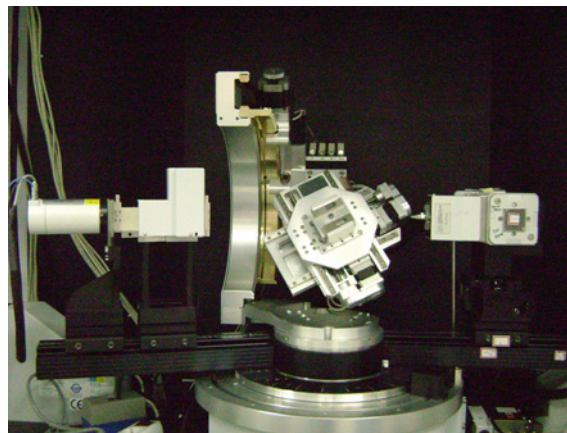Figure 8: Texture goniometer at Indian Institute of Science, Bangalore.

Table 1: Comparison of various radiations used in materials characterization.

	Light	Neutrons	X-rays	Electrons
Wavelength (nm)	400–700	0.05–0.3	0.05–0.3	0.001–0.01
Energy (eV)	1	0.01	10^4	10^5
Charge (C)	0	0	0	$-1.602 * 10^{-19}$
Rest mass (g)	0	$1.67 * 10^{-24}$	0	$9.11 * 10^{-28}$
Penetration depth, Absorption length (mm)	–	10–100	0.01–0.1	10^{-3}

method described above have disadvantages of their own and it lead to spurious intensities called ghosts. In order to overcome this inherent drawback of spherical harmonic methods, discrete or direct methods like WIMV (Williams-Imhof-Matthies-Vinel) [12] and Arbitarily Defined cells (ADC) [13] have been developed to calculate ODF from the measured pole figures.

The three Euler angles (the way they are obtained) and three-dimensional view of the Euler space is presented in Fig. 7(a, b). In the figure, the location of the technologically important {111} fibre (fibres are loci of orientations with common plane or common direction) as well as some important ideal orientations are shown. A two-dimensional $\Phi_2/Phi = 45°$ section (Bunge and Roe notation respectively), in which a few ideal orientation are identified, is displayed in (Fig. 7(c) and (d)). The availability of ODFs has made possible the quantitative comparison of textures; furthermore, the higher resolving power associated with ODFs has enabled researchers to recognize more clearly many details of individual textures which may be smeared out and difficult to read in a pole figure. It is to be mentioned, however, that in spite of the limitations, pole figures still remain the most popular way of representing texture. In this review, for readers' convenience, all the textures will be described in terms of pole figures.

3. Measurement of Textures
The texture associated with polycrystalline materials is a crystallographic feature in global sense. Therefore, all crystallographic measurement tools can be effectively used to measure texture with adequate modification in instrumentation. Many methods have been used to determine texture. In fact, all most all the diffraction techniques are used to measure crystallographic texture. However, texture analysis is mostly popularly carried out by polycrystal diffraction using X-rays, neutrons or electrons. The basis of texture measurement is as follows. The intensity of any diffraction peak depends on the volume fraction of crystals which are in diffraction position in the considered

sample direction. Hence the intensity ratios of the diffraction peaks are a first (qualitative) indication of the texture of the material irradiated. In the initial stages of texture research, the intensity variations in Debye–Scherrer photographs were taken as representative of texture variation in a qualitative manner. The next step was to combine several such photographs, taken for different sample positions, and the results of all these measurements were depicted through stereographic projections, however, these remained still qualitative. Ever since X-ray detectors have been introduced, semi-quantitative measurement of texture through pole figures became possible, and this remains the most popular method till date.
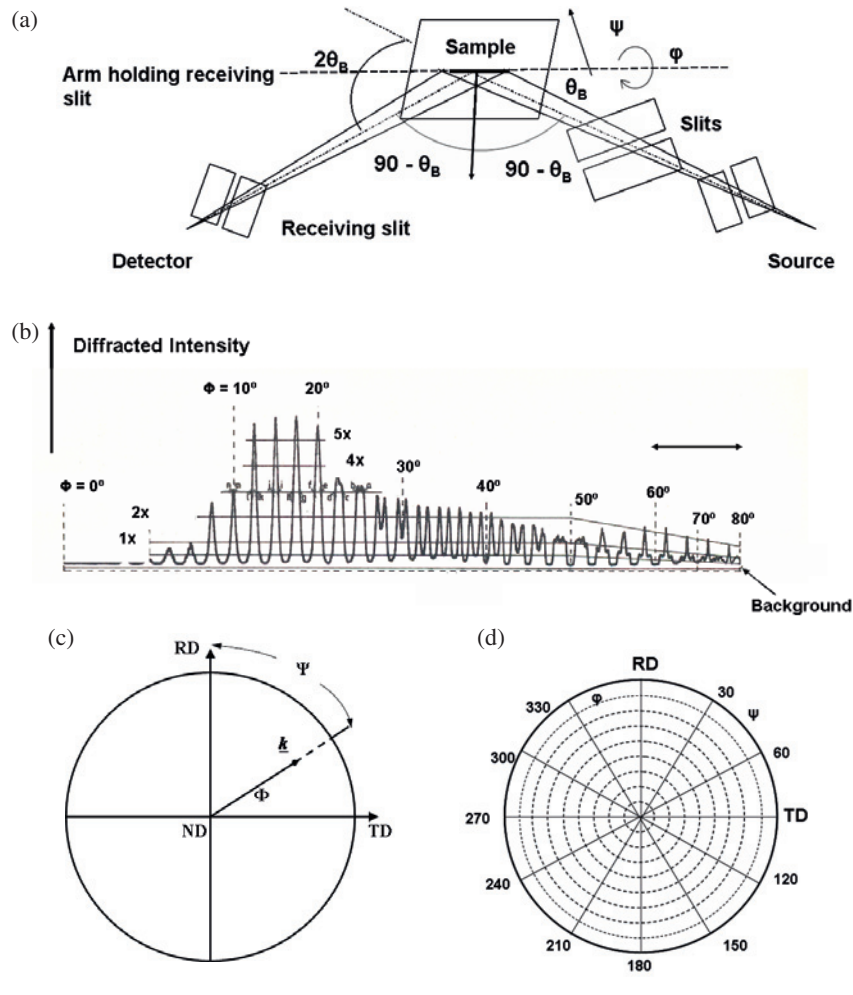
The second highly used method is based on electron back scatter diffraction (EBSD) [14–15] in scanning electron microscope (SEM). For selective purposes, neutron diffraction [16–17] on synchrotron X-rays [18] are also used for texture measurement. Each of these methods have their advantages and limitations for a given research problem due to a characteristic radiation and its interaction with matter. Table 1 represents some characteristics of these radiations. All these methods will be described in brief in the following sections.

3.1. X-ray Diffraction
X-ray diffraction is the oldest and still the most popular method for texture measurement. It was first employed by Wever [19]. However, since then the method has made a great advancement. Current day x-ray texture goniometer uses the geometry by Schulz [7] and is equipped with electronic detectors. Fig. 8 shows view of the X-ray texture goniometer at Indian Institute of Science. The principle of texture measurement using Schulz method is as follows:

In order to determine the orientation of a given lattice plane (hkl), the diffractometer is first set to the adequate Bragg angle, (θ_B) of the diffraction peak of interest. The sample is rotated in a goniometer until the lattice plane (hkl) is bought in reflection condition (i.e. the normal to the lattice plane or diffraction vector is the bisectrix between incident and diffracted beam Fig. 9a). In the case

of a polycrystalline sample, the intensity recorded at a certain sample orientation is proportional to the volume fraction of crystallites with their lattice planes in the given reflection geometry. In order to correlate the intensity of the diffracted beam from a particular location with the overall geometry of the specimen, the sample is allowed to rotate (ψ) about an axis normal to the irradiated surface. This is repeated for different sample tilt (Φ).

Determination of texture can be done on a sample of large thickness and a plane surface on which x-rays are reflected, or on a thin slab which is penetrated by X-rays. Because of defocusing effects as the flat sample surface is inclined against the beam, variations in the irradiated volume and absorption intensity corrections are necessary, particularly in reflection geometry. In reflection

geometry, only incomplete pole figures can be measured, usually to a pole distance of 80° from the sample surface normal. The schematics of texture measurement are depicted in Fig. 9(a–d).

Conventional texture goniometers are equipped with a single detector, e.g. a scintillation counter, the receiving slits of which are chosen in such a way that the total integrated intensity of the chosen Bragg-peak is registered [20]. This requires rather broad slits in order not to cut off and parts of the Bragg peak especially at higher sample tilt angles. This method works quite well with materials the diffraction spectra of which contain only a low number of well-separated peaks. On the other hand, if the number of diffraction peaks is higher, and their angular distance is smaller, they may overlap even at low or moderate tilt angles. In some cases, it

Figure 10: (a) Principle of one dimensional location sensitive overflow, overpressure gas ionisation counter (b) Pole figure measurement with a position sensitive detector (PSD) [22].
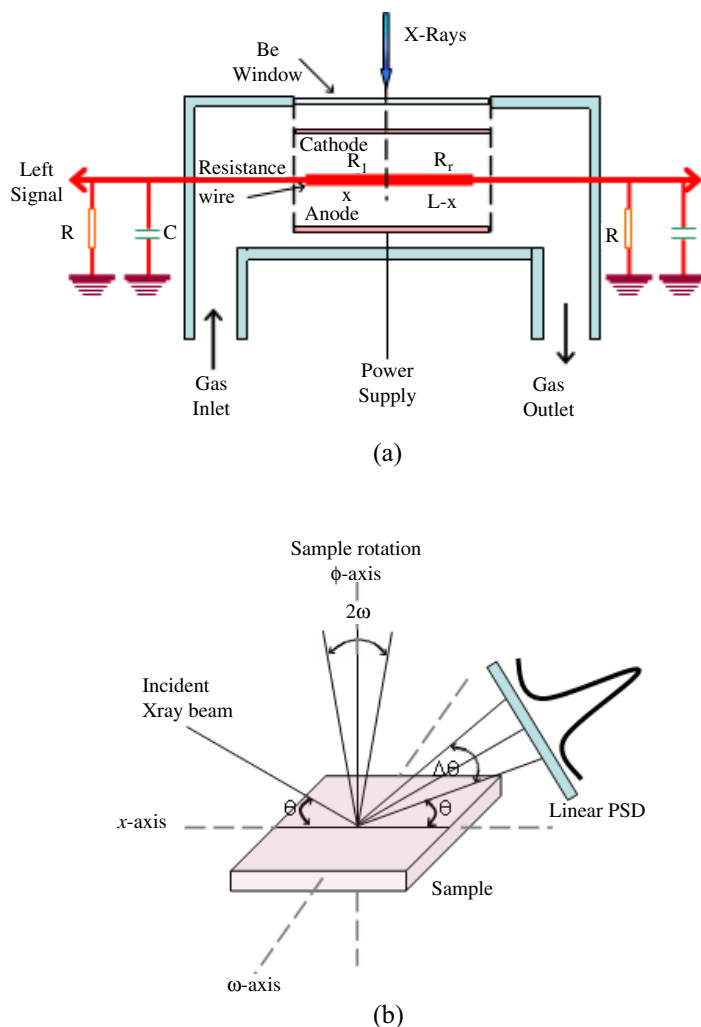
is then still possible to use this method with smaller receiving slits, taking into account that part of the broadened peak might get cut off at higher tilt angles. This error gets corrected with the help of defocusing correction which can be determined in a random sample. However, this method has its limitations in more complex diffraction spectra, e.g. in ceramics or geological materials. In such cases, it is necessary to measure the complete diffraction spectrum for each pole figure point and to apply a de-convolution procedure in order to separate the increasing peak overlap with increasing tilt angle. This is done with small receiving slits, which increases the measuring time considerably. At the same time, these materials often show also lower diffraction intensities. Due to lower crystal symmetry, the number of required pole figures for complete texture determination is higher. The necessary measuring times would thus be quite high. This situation can be improved by using a position sensitive detector (PSD) which measures the diffracted intensities in a whole 2θ-range simultaneously. Position sensitive detectors (PSD) are proportional counters that use gas ionization and a localized electron-avalanche process to amplify the signal from a detected X-ray (Fig. 10). Both linear (1-D) and area (2-D) type position sensitive detectors (PSD) are available. Linear position-sensitive detectors use a fine wire to collect intensity over an angular range simultaneously, offering speed advantages up to one hundred times that of a point detector (scintillation and solid-state). These PSDs may be held fixed over a 5 to 10 degree 2-theta range, or scanned like a point detector over a larger range.

Figure 11: Schematic of Time of Flight (TOF) measurement in Neutron Diffraction [22].
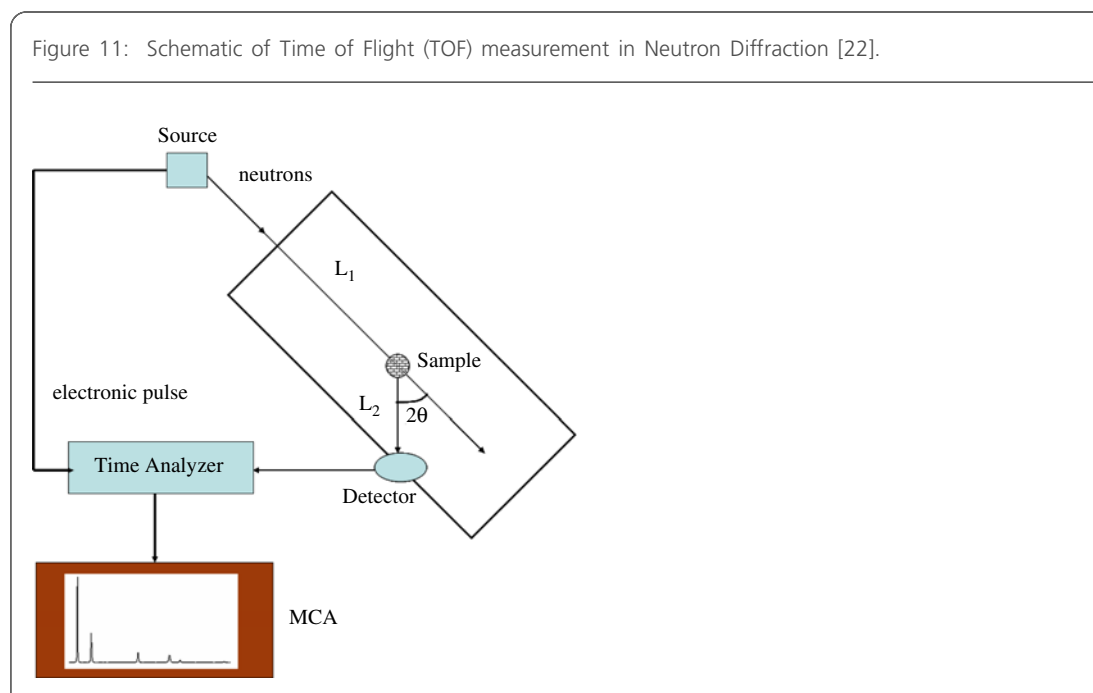
The speed of this detector is advantageous for high sample throughput, time-resolved studies, weakly diffracting materials, and the detection of minor phases.

Pole figure measurement using a two-dimensional area detector allows an angular resolving power $\sim 0.1°$ in 2θ such that texture analysis in "advanced materials" with peak-rich diffraction diagrams is possible. Combined with an appropriate step scanning regime angular resolution in the pole figure angles of the same order of magnitude can then be obtained if a small enough aperture of the primary beam is used. This method is applicable to very sharp textures, e.g. epitaxial layers on single crystalline substrates, and to "multipeak textures" in which a large number of crystallites can be individually resolved. The method has been particularly useful in connection with quantitative mathemathical models of texture formation and to the study of behaviour of individual crystallites in the environment of a polycrystalline aggregate.

High temperature texture measurement set up [21] also has been developed for *in situ* measurements of texture. This is quite helpful to study texture evolution during heating and cooling, therefore providing a deeper understanding of texture formation during phase transformations.

3.2. *Neutron diffraction*
Texture measurement by neutron diffraction is a very powerful technique for overall texture analysis. However, by virtue of the fact that it requires nuclear reactors with a constant flux

of thermal neutrons, or with pulsed neutrons at spallation sources, it is not so commonly used. It was first applied for the determination of magnetic structure in steel. The wavelength distribution of thermal neutrons has a broad spectrum with a peak at 1–2 Å, similar to X-rays. A disadvantage of neutron is that the interaction of neutrons with matter is weak, therefore, long measurement time is required. However, this could be an advantage also as it provides high penetration and low absorption, making neutrons suitable for bulk texture investigations of large sample volumes. Texture measurement by neutron diffraction also provides an additional advantage, because of the low absorption; in situ measurements involving texture changes during heating, cooling or in-situ deformation are carried out with great accuracy. Neutrons are also sensitive to measuring the orientation of magnetic dipoles. Therefore, magnetic pole figures can be determined with some limitations. A conventional neutron texture measurement at a reactor source uses monochromatic radiation produced with single crystal monochromators. The sample is rotated by a goniometer to cover the entire orientation range, analogous to an X-ray texture goniometer. To improve counting efficiency, *position-sensitive detectors* have been applied, similar to X-ray based measurement techniques. In recent times, with the advent of pulsed neutron sources it has become customary to use *polychromatic* neutrons and detector system that can identify the energy of neutrons by measuring the time of flight (TOF). This

Figure 12: Schematics of Synchrotron Texture measurement [140].
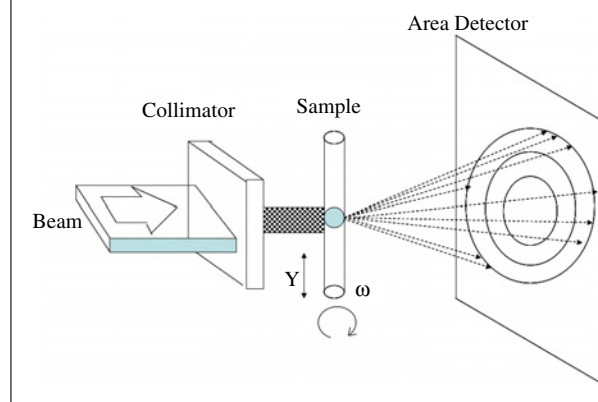
is based on the principle that flight time of neutron is a measure of energy or wavelength of neutrons. In the diffracted beam, the detector signal is stored in a multi channel analyser synchronously with each neutron pulse. The recorded spectrum is successively built up corresponding to the neutron flight time, for example, first signal that corresponds to the fastest (high energy/low wavelength) neutrons are stored in the first channel and so on. The principle of time of flight measurement is shown in Fig. 11. The details of this method can be found in the text of Kocks, Tome and Wenk [9].

3.3. *Synchrotron X-rays*
The intensities produced by conventional X-ray tubes are typically low. In addition, the beam used for irradiation is too wide, nearly a millimeter. In contrast a synchrotron produces a very fine-focused high-intensity beam of x-rays. These high intensity beams can be used for texture measurement as these would penetrate deeper in the material. The small beam size nearly less than 5 μm is an additive plus, as one can selectively obtain information from desired volume. Diffraction patterns from synchrotron are recorded by CCD detectors. Therefore, their instantaneously display the presence of texture expressed in systematic intensity variations along Debye rings. Texture is immediately recognized as intensity variations along Debye rings in diffraction images, yet in many cases this information is not used because the quantitative treatment of texture information has not yet been developed into a standard technique. Fig. 12 presents the schematic illustration of a synchrotron texture measurement.

In Fig. 12, geometry of a transmission diffraction experiment is shown on a heterogeneous sample. If the sample is stationary, the diffracting planes will be inclined by an angle $(90° − \theta)$ to the incoming beam. Therefore, the corresponding reciprocal lattice vectors lie on a cone with an opening angle of $(180° − 2\theta)$, which intersects the orientation sphere of the sample in a small circle. Coverage of the pole figure from a single image is minimal but even information from such an image can be sufficient to determine the orientation distribution and then to reconstruct complete pole figures. The use of high energy is advantageous because of good penetration and moderate absorption, as well as small 2θ angles.

The wide availability of X-ray area detectors facilitates the application of synchrotron radiation based X-ray diffraction for the determination of texture. These measurements are very fast compared to other techniques. In special cases, it is possible to interpret the texture information contained in these intensity variations intuitively. However, diffraction studies focused on the effects of texture on materials properties often require the full orientation distribution function (ODF) which can be obtained from spherical tomography analysis. In cases of high crystal symmetry (cubic and hexagonal) an approximation to the full ODF can be reconstructed from single diffraction images. Combined with area detectors, the reconstruction methods make the measurements fast enough to study orientation changes during phase transformations, recrystallization and deformation *in situ*, and even in real time, at a wide range of temperature and pressure conditions. Synchrotron analysis is particularly valuable for compounds with weak scattering (e.g. polymers and biological materials) and for investigating local texture variations.

3.4. *Scanning electron microscope – Electron Back Scatter Diffraction (SEM-EBSD)*
In recent time, this technique is probably the most popular technique for texture measurements due

Figure 13: (a) Schematics of EBSD measurement set up, (b) Schematics of formation of Kikuchi bands in EBSD [22].

(a)   (b)
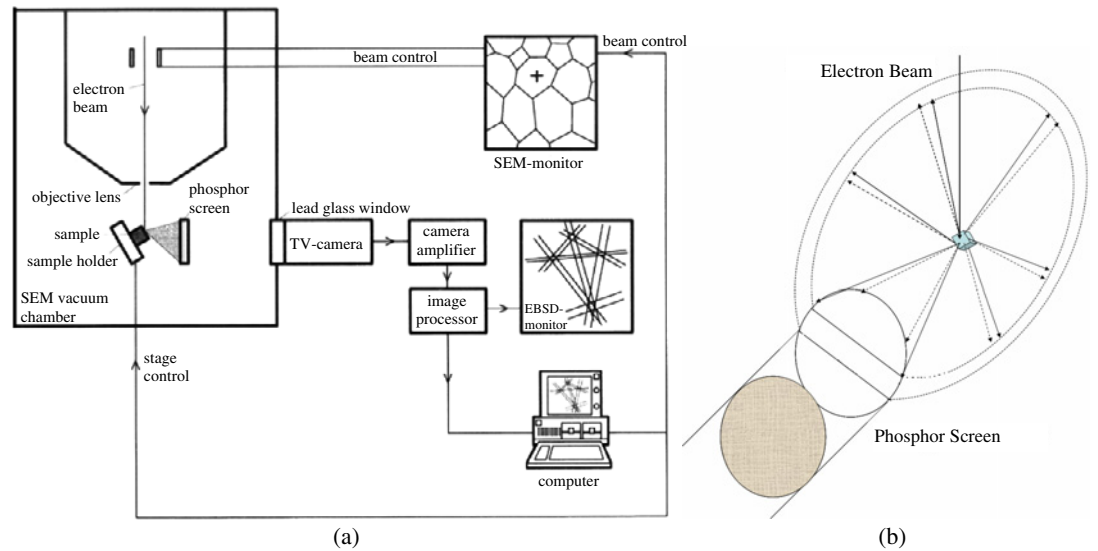
Figure 14: Schematic representation of the orientation imaging system used in [30].
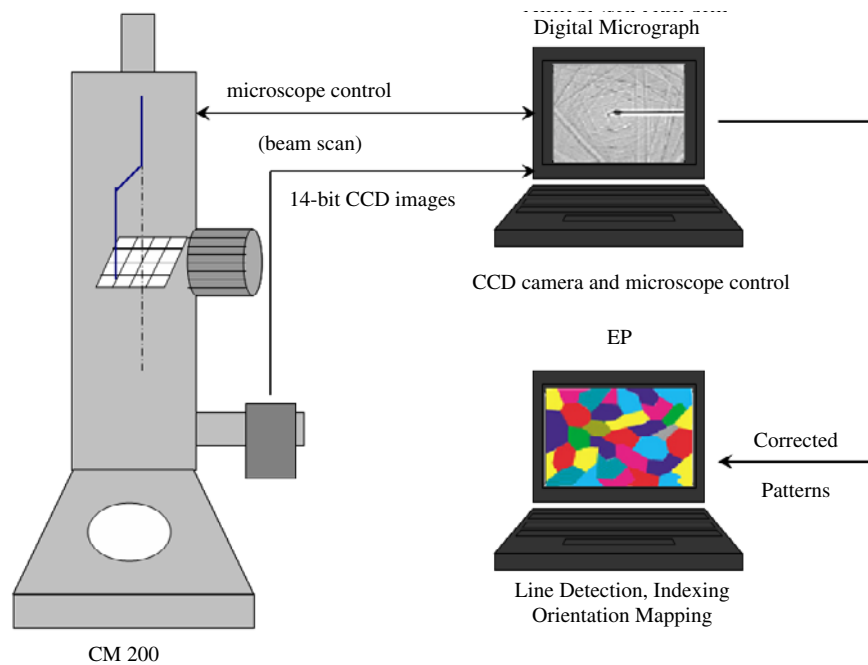
to the easy availability and operation of scanning electron microscope (SEM) plus it does not require much background in texture theory from the user. In the SEM-EBSD method, the interaction of the electron beam with the uppermost surface layer of the sample produces electron back-scatter diffraction patterns (EBSD) that are analogous to Kikuchi patterns in the TEM. These patterns are captured on a phosphor screen and recorded with a low intensity video camera or a CCD device. The beam is made to scan the area of interest and in case of large area scans, the sample can

be translated using a high precision mechanical stage in increments as small as 0.1 μm or even lower. At each position a pattern is recorded. The digital signal is then fed to a computer and indexed using Hough transform. Specimen coordinates, crystal orientation, parameters describing the pattern quality and a parameter evaluating the pattern match are recorded. Then the beam is translated to the next position and the procedure is repeated. A spatial resolution of less that 0.1 μm can be reached on a SEM equipped with a field emission gun. A schematic view of SEM-EBSD system and the working principles are shown in Fig. 13. The biggest advantage of EBSD is that it is the only technique that provides localized texture information in a quantitative manner as against TEM. It thus helps in bridging the gap between bulk texture measurement techniques like X-ray and localized TEM technique. This method is rigorously and adequately described in the text due to Randle and Engler [22].

This sounds like an ideal technique. However, it is only applicable to crystals with fairly low dislocation densities (of course, in recent times, this limitation has largely been overcome due to advent of field emission gun microscopes), surface preparation is critical and the automatic indexing procedure is not always reliable. Failure to index and mix-indexing of patterns are both orientation dependent and can produce texture artifacts. Further more, there are statistical limitations.

3.5. *Transmission electron microscopy –*
Orientation imaging microscopy (TEM-OIM)

Transmission electron microscopy (TEM) is probably one of the most accurate methods for texture measurement, however, at a local scale. TEM not only provides information about orientation but also about grain shape and, more importantly, about dislocation microstructures indicative of active deformation mechanisms. There are several methods to determine crystal orientations from transmission electron microscope (TEM) electron diffraction patterns. The oldest and frequently used technique is to analyze the spot diffraction patterns. It has been practiced by many researchers for a long time to use selected area diffraction (SAD) in polycrystals to get a rough idea of the misorientation of crystals in the illuminated area. Schwarzer [23–24] proposed a method to get pole figures in the TEM by recording the diffracted intensity in SAD as a function of the specimen orientation. However, the correlation between the orientation and the precise spatial location is lost in this technique. There are commercially available packages that use 'dark field scanning' to generate orientation-based microstructure maps.

In this case, the orientation of a point (pixel) in the image is determined from intensities obtained for various incident beam directions. However, for all the methods based on spot diffraction patterns, the orientation accuracy is low. Even if the indexing procedure takes into account the intensity of diffraction spots, the accuracy is not up to the desirable extent [25–26]. Kikuchi patterns have been used for orientation determination for a long time [27] and orientation maps based on Kikuchi patterns in TEM have been reported [28–29]. Analogous method based on Kikuchi patterns or convergent beam electron diffraction (CBED) patterns can be applied for getting orientation maps on transmission microscopes. Recently, a set up developed by Fundenberger et al. [30] has made texture determination by TEM based orientation mapping very accurate and handy. Contrary to what was often claimed in the past, the sample thickness is not really a limitation for applying this method. Even for thin samples, at least CBED patterns can be obtained. The schematic of texture measurement in a TEM and corresponding data acquisition and analysis is shown in Figures 14 and 15.

In addition, textures are also determined by ultrasonic wave propagation [31]. Directed ultrasonic velocity measurements predict texture by taking advantage of the effects of directionality (anisotropy) that exists in the material. Measurement technique uses the angular variation of the ultrasonic waves in the material to detect texture and directionality (Fig. 16). The effect of texture on velocity of the ultrasonic wave is to slow it down in one direction and make it faster in another. Ultrasonic velocity measurements take advantage of this effect, thus determining texture parameters like "C" coefficients.

4. Texture in Metals and alloys
4.1. *Sources of Texture in metallic materials*

Texture evolves or gets modified at almost every stage of processing. In fact it is very difficult to avoid texture completely at any stage of materials processing. The metal castings have a very clear and characteristic texture which depends on material, purity as well as solidification conditions. However, in most of the cases, these textures are modified in subsequent stages of processing. The most important development of texture takes place during plastic deformation, and recrystallization following such deformation. It is well known that the orientation of the axis of a long metallic single crystal rotates when it is plastically deformed in tension [32]; the axis rotates towards the slip vector and the slip planes become progressively more nearly parallel to the tensile axis. When slip begins on

Figure 15: CBED patterns before and after image correction from [30]: (a) raw CBED pattern in which deficient lines are visible inside the transmitted beam and excess lines outside; (b) corrected CBED pattern, the lines are enhanced, but one can also see that the contrast can change along a line; and (c) indexed CBED pattern.
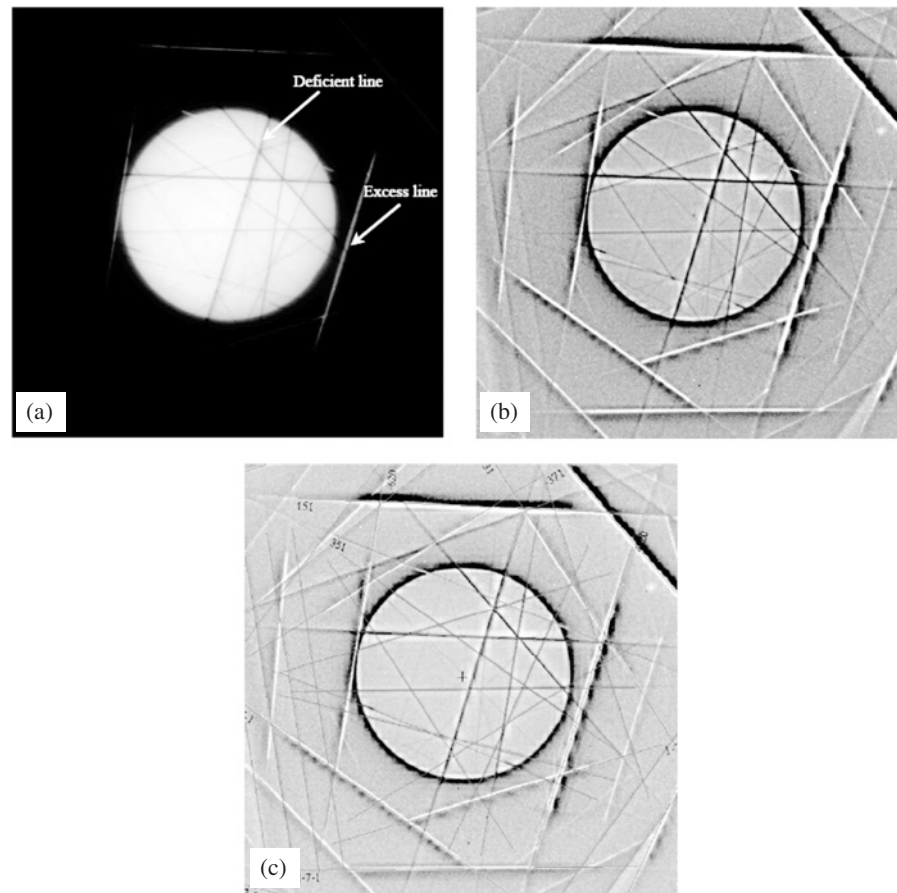

two planes simultaneously, the rotation is abruptly slowed and its character changes. In a polycrystalline aggregate, the individual grains behave in an analogous way. However, during deformation the grains of a polycrystal are more severely constrained than a free single crystal, as each grain has to fit in with the overall strain of the aggregate. The problem of polycrystal deformation and resulting evolution of texture has been addressed very intelligently by Taylor [33], based on von Mises' [34] criteria that individual grains require the operation of at least 5 independent slip systems to achieve an arbitrary imposed strain. Taylor introduced a criterion of minimum work: that combination of 5 systems, out of the many possible combinations, will function which minimizes M, the Taylor factor. The Taylor factor is given by:

$$M = \frac{\sum_{\alpha} d\gamma^{(\alpha)}}{d\varepsilon}$$

where $d\gamma^{(\alpha)}$ is the shear on α^{th} slip system and $d\varepsilon$ is the macroscopic tensile or compressive strain. Since then several improvements have been carried out on the original proposition of Taylor. The most important work was due to Bishop and Hill [35–36], who suggested that the Taylor theory satisfies the yield criterion. i.e., that the shear stress reaches the critical level for slip on the active systems identified by Taylor without exceeding it on the inactive slip systems. The Taylor–Bishop–Hill (TBH) theory assumes strain continuity from one grain to its neighbors, i.e., each grain deforms as the assemblage does. But this assumption is incompatible with stress, as the von Mises' criteria that at least 5 slip systems are required in each grain also becomes unsustainable. Later Fleischer [37] had shown that in polycrystalline α-brass, some grains show four or even fewer distinct slip systems.

The evolution of annealing textures by recrystallization of deformed polycrystal has been

Figure 16: Principle of Ultrasonic measurement.
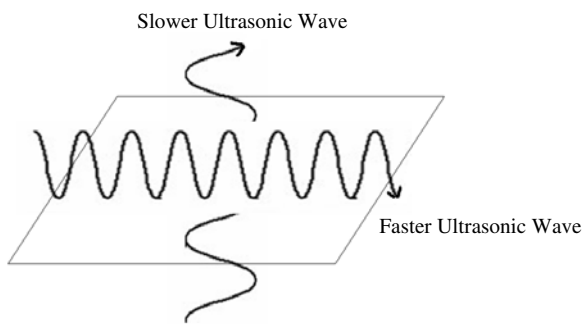
widely investigated; however, a general theory that could explain the evolution of so-called recrystallization textures is still awaited. For almost three to four decades, two school of thoughts [38–41] prevailed in this area. The first of them assumes that annealing textures are formed by oriented nucleation, i.e., the creation of nuclei by the formation of a recrystallized nucleus in a particular orientation relationship to the region of a deformed grain in which it appears. Much of the evidence in support of this model comes from microscopic studies, both by transmission electron microscopy (TEM) [42–43] as well as orientation imaging microscopy (OIM) studies [44–45]. The other school of thoughts believed that nuclei are formed at random, but only particular orientations among all these nuclei are capable of growing rapidly at the expense of other nuclei.

Of late, a third school of thoughts [45–46] has come into existence, which is based on strain–energy maximization. The model originates from the presumption that the stored energy due to dislocations is the major driving force for the recrystallization. In this model, the absolute maximum internal stress direction due to dislocations generated during deformation in the material is aligned with the minimum Young's modulus direction in recrystallized grains, whereby the energy release during recrystallization can be maximized. The proposers of this theory argue that material does not change its shape and volume macroscopically during recrystallization, and therefore, recrystallization is a displacement controlled process. The absolute maximum internal stress direction may be obtained from the operating slip systems, which are related to the deformation mode and consequently the deformation texture. For example, if one slip system is activated, the absolute maximum normal stress direction is parallel to the slip direction, or the Burgers vector

direction. If more than one slip system is activated, the absolute maximum normal stress direction can be determined by the vector sum of related slip directions, taking their contribution to slip into account.

Variables such as alloy composition; trace impurities; presence of a second phase; degree, mode and temperature of deformation; differences between surface and interior layers; annealing temperature; thermal history before annealing; rate of heating to temperature — all these play a role in determining texture.

4.2. *Textures of FCC Metals and Alloys*

The nature of slip in face-centered metals and alloys, particularly, is strongly affected by the stacking fault energy (SFE) [47], more correctly the specific SFE (γ/Gb) [48] which is related to the partial dislocations in a dissociated perfect dislocation. This energy (SFE) in turn has a strong effect on both wire and sheet textures. Fig. 17 shows this very clearly with respect to rolling textures in Nickel as a function of Cobalt addition [49]. It is well known that cobalt addition decreases SFE of nickel. Similar effects are familiar in relation to wire drawing.

In general, two types of rolling textures are recognised in FCC metals and alloys; namely Copper or Metal type texture and Brass or Alloy type texture (Fig. 18). These textures are named after the metal and the alloy in which they were observed for the first time. In general, a Copper type texture consists of orientation named Copper (Cu) {112} <111>, S component {123} <634>, and Brass (Bs) {110} <112> plus some other minor components. The Brass type texture is characterized by ideal orientation {110} <112>, {123} <634> plus a minor {110} <001> component. The rolling texture of materials with high to medium stacking fault energy are characterized by Copper type texture while the low stacking fault energy materials possess Brass type texture. Results from a number of quantitative texture studies indicate that the textures of most FCC metals (except silver) are of the copper type, whereas those of silver and most FCC alloys are of the brass type.

Extensive work has been done in order to determine the recrystallisation texture of such polycrystalline FCC metals as copper, aluminium and nickel and their various alloys [50–52]. Annealing of such rolled sheets can produce an annealing texture that mimics the deformation texture; generate one or more quite new textures; produce approximate randomness; or generate the extraordinary cube texture. As in the case of deformation textures, the most completely documented material is copper and its alloys. The

Figure 17: {111} Pole figures showing the rolling textures of: (a) pure Ni; (b) Ni-10% Co; (c) Ni 20% Co; (d) Ni 30% Co , (e) Ni 40% Co; and (f) Ni 60% Co [49].
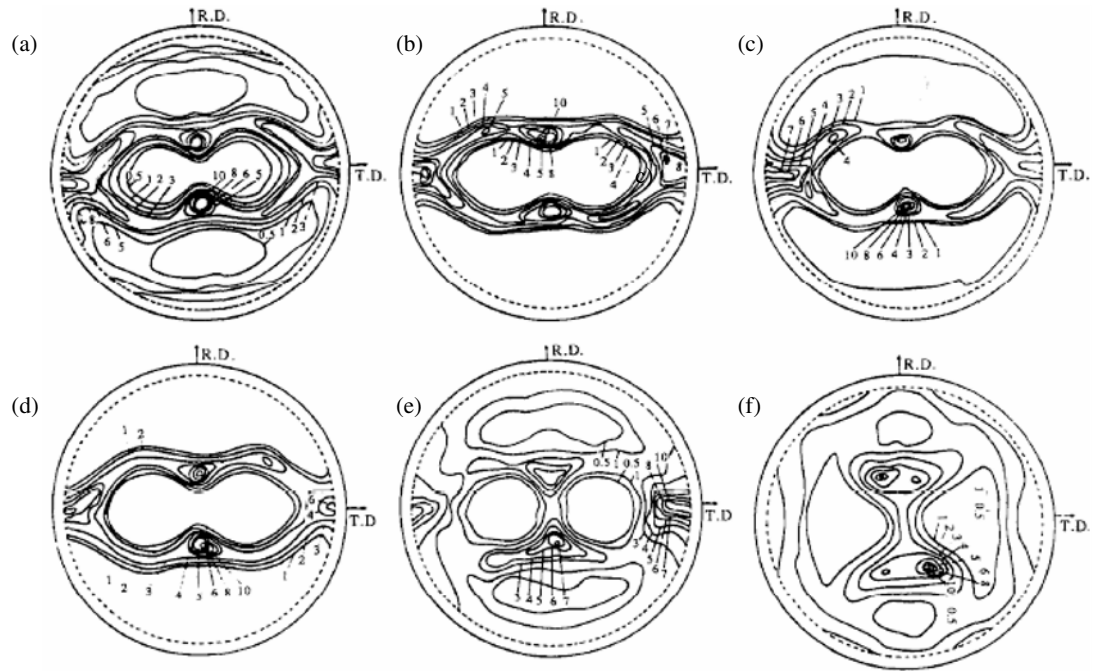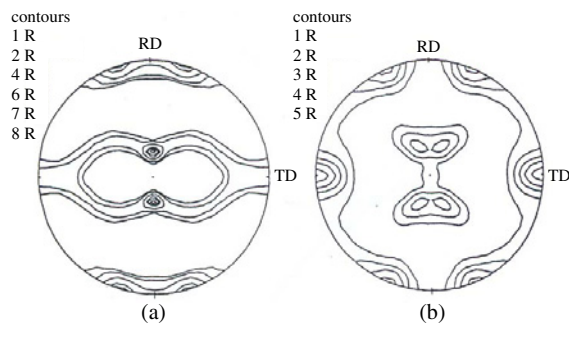
Figure 18: (111) pole figure for 95% rolled (a) Copper (b) 70:30 Brass.

particularly sharp cube texture, {100} <001>, which is found in recrystallisation texture of high to medium stacking fault energy materials is of both practical and scientific interest (Fig. 19). A large number of investigations have been carried out into the formation of annealing textures of aluminium and its alloys as well as copper.

It has been found that heavy strain and a small penultimate grain size favours formation of cube texture in copper, while mode of deformation like cross rolling etc., some alloying elements, even in trace quantities, especially those that cause strong solution-hardening, prevent its formation. Although cube textures have been rigourously dealt in the context of FCC metals and alloy, they can also form in steels as well. The cube grains form in narrow transition bands which separate principal components of the deformation texture.

For aluminium of 99.99% purity and above [53], it is rather more difficult here to produce 100% cube texture. For prior deformations of 90% and above, the recrystallisation texture consists usually of a cube component plus a component described variously as 'retained rolling texture' and the 'S

Table 2: Important FCC rolling texture components and their location in Euler space.

Name	Indices	Bunge (Φ_1 Φ Φ_2)	Kocks (Ψ Θ φ)
Copper	{112} <111>	90, 35, 45	0, 35, 45
S1	{124} <211>	59. 29, 63	149, 28, 27
S2	{123} <412>	47, 37, 63	137, 37, 27
S3	{123} <634>	59, 37, 63	149, 37, 27
(commonly referred as S)			
Brass	{110} <112>	35, 45, 0	55, 45, 0
Taylor	{4 4 11} <11 11 8>	90, 27, 45	0, 27, 45
Goss	{110} <001>	0, 45, 0	90, 45, 0

Figure 19: Depiction of crystal arrangements for (a) a randomly textured and (b) a strongly cube textured material and corresponding (111) pole figure.

(a)   (b)
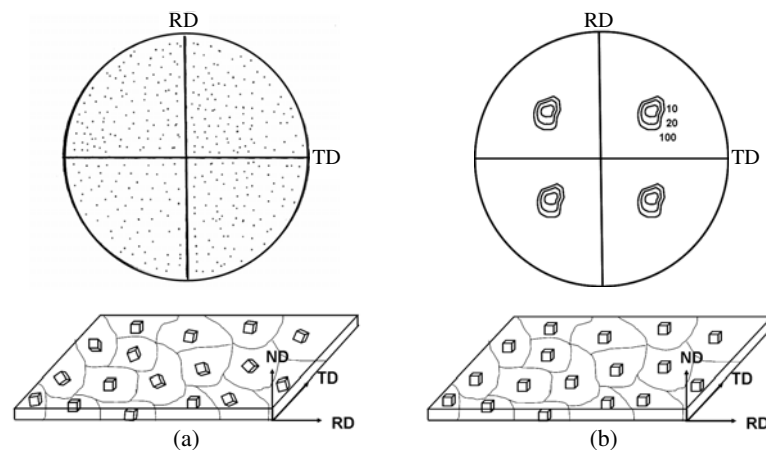
texture'. As may be inferred from the designation, this later component is similar to the main rolling texture component for aluminium (called the 'R texture'). The amount of the cube component in the annealing texture of pure aluminium can be increased by prolonged annealing or by raising the annealing temperature. It has been found that the cube texture in aluminium is favoured by a well-developed rolling texture and a high annealing temperature.

4.3. *Texture of BCC metals and alloys*
Most of the work on the deformation textures of BCC metals and alloys has been concentrated on steels, specially low and extra low carbon steels [54–56], because of their industrial importance. Out of the various applications of these steels, the most important one has been for the purpose of deep drawing of cold rolled and recrystallised steel sheets. The major texture components in deformation of BCC metals and alloys are the α fibre {001} <110> to {111} <110> (appears in the $\phi_1 = 0°$

and 90° sections of the ODF) and γ fibre {111} <110> to {111} <112> (visible in $\phi_2 = 45°$ section of the ODF Fig. 7b). Table 3 shows the position of important texture components observed in rolling of BCC materials in the Euler space. Fig. 20 shows experimentally measured (200) pole figure for low carbon steel and the orientation of fibres in the same pole figure. The other important fibers in bcc metals and alloys are η fibre from {001} <100> to {011} <100>; ε fibre from {001} <110> to {111} <112> and β fibre from {112} <110> to {11 11 8} <4411>. It is generally observed that there is a shift in intensity from {001} <110> to {112} <110> on the α fibre and from {111} <112> towards {111} <110> on the γ fibre, as the amount of cold work increases.

Optimization of appropriate texture is very crucial for sheet products, especially steels used for deep-drawing. The deep drawability of a sheet material is its capacity to achieve a high degree of plastic flow in the plane of the sheet, while offering sufficient resistance to flow in the thickness direction.

Figure 20: Rolling texture of low carbon steel from (200) pole figure after 90% reduction b) partial fibre textures commonly used to describe rolling texture [1].
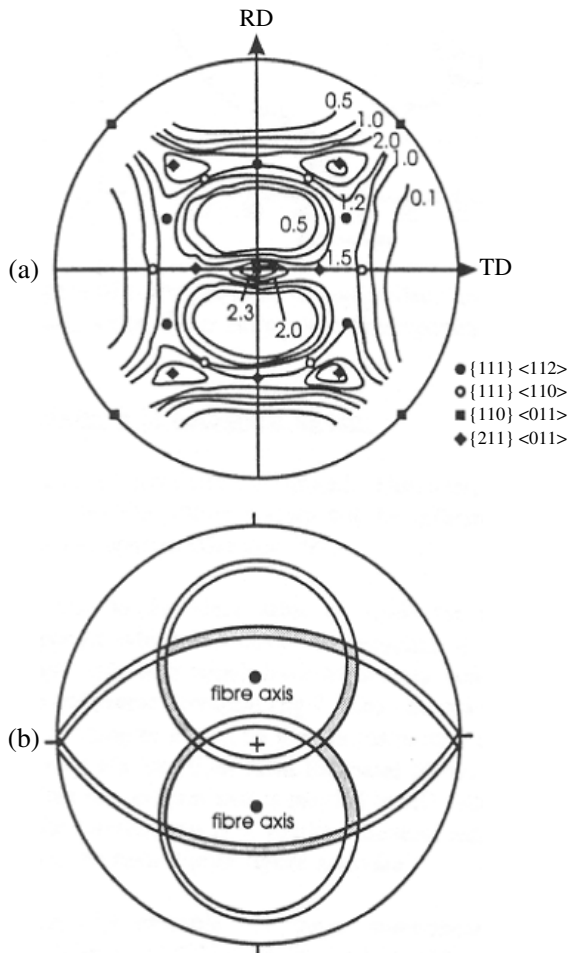

(a)

(b)

- ● {111} <112>
- ○ {111} <110>
- ■ {110} <011>
- ◆ {211} <011>

Table 3: Rolling texture components in BCC metals.

{h k l}	<u v w>	Φ_1	Φ	Φ_2
001	110	45	0	0
211	011	51	66	63
111	011	60	55	45
111	112	90	55	45
11, 11, 8	4, 4, 11	90	63	45
110	110	0	90	45

This property of a material is called the "normal anisotropy" and is commonly evaluated in terms of the r_m (also called $\bar{r}$) or average r-value. This is defined by the relationship $r_m = (r_0 + 2r_{45} + r_{90})/4$, where the subscripts 0, 45 and 90 refer to inclinations of the longitudinal axes of sheet tensile test pieces to the rolling direction of the sheet, and each individual

r-value is the ratio of width strain/thickness strain, as measured in a simple tensile test. The "planar anisotropy", Δr has been defined as follows: $\Delta r = (r_0 + r_{90} - 2r_{45})/2$. This is a measure of the tendency for ear forming during the deep drawing operation. It is clear from the above that in order to be highly deep drawable, a sheet material should have as high a value of r_m and as low a value of Δr, as is practicable. It has been demonstrated that high normal anisotropics as r_m values are displayed by materials which have a high proportion of grains oriented with their {111} planes parallel to the sheet plane; i.e., by materials which possess a strong {111} type texture. Other texture components, such as the {001}, have been found to be detrimental to the drawability and, in practice the intensity ratio of the above two components, $I_{\{111\}}/I_{\{001\}}$, is found to be approximately linearly related to r_m.

4.4. Texture of HCP metals and alloys

Texture in hexagonal structural materials has attracted significant interest over the years because of the use of zirconium alloys like Zircaloy for cladding of nuclear reactor fuels [57–58], titanium alloys for structural materials in aerospace and aircraft industry [59–61]. From deformation mechanistic point of view, HCP metals are quite different from cubic metals. In these metals, limited slip systems are available and twinning plays a significant role in deformation and therefore texture evolution. The deformation model in hexagonal crystals is based on the following three distinct slip systems and two twinning system: (i) basal $\{0\,0\,0\,1\} <1120>$ (ii) prismatic $\{10\bar{1}0\} <11\bar{2}0>$ (iii) pyramidal $\{1\,1\,\bar{2}\,2\} <11\bar{2}3>$ and $\{1\,0\,\bar{1}\,1\} <11\bar{2}0>$; as well as (iv) compressive $\{\bar{2}\,1\,1\,2\} <\bar{2}\,1\,1\,3>$ and (v) tensile $\{1\,0\,\bar{1}\,2\} <10\bar{1}1>$ twinning. The formation of deformation texture in HCP metals and its alloys will develop in accordance with the relative contributions from the above deformation processes. It is observed that the slip plane will gradually rotate toward the rolling plane and the slip direction toward the rolling direction.

The characteristics of deformation texture in hexagonal materials with different c/a ratios are crudely classified into three groups. The tendency is that (i) the basal $\{0\,0\,0\,1\} <1120>$ slip will result in the basal texture for Mg ($c/a \approx 1.633$); (ii) the combination of basal $\{0\,0\,0\,1\} <1120>$ slip and pyramidal $\{1\,1\,2\,2\} <1123>$ slip will result in the textures with basal poles tilted away from the normal direction toward the rolling direction for Zn or Cd ($c/a > 1.633$); and (iii) the combination of prismatic $\{1\,0\,.1\,0\} <1120>$ slip and basal $\{0\,0\,0\,1\} <1120>$ slip will result in the textures with

Figure 21: Rolling Texture (0002 pole figures) of HCP metals with different c/a ratio (a) Magnesium with c/a ideal shows basal texture (b) Zinc with c/a > ideal shows 15–25° shift from basal towards RD (c) Titannum with c/a < ideal shows 20–40° shift from basal towards TD [1].
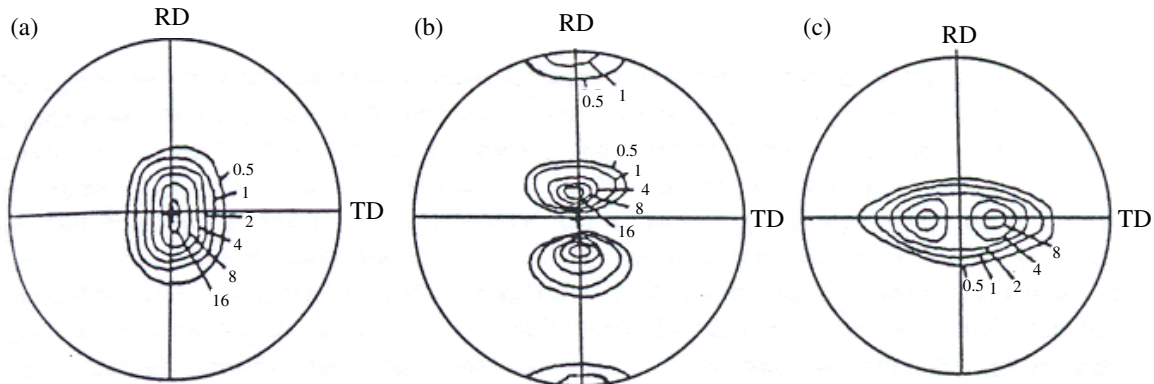
Table 4: Texture development in different HCP metals and alloys for a variety of processing steps [62].

Material	Processing	Major Texture Components
Cd and Zn	Columnar solidification	$<01\bar{1}0>$ fiber texture
Mg	Columnar solidification	$<01\bar{2}0>$ fiber texture
HCP metals and alloys	Wire and rod manufacture	$<01\bar{1}0>$ fiber texture
Metals with $c/a > 1.623$ (Zn, Cd)	Cod rolling	$\sim\{11\bar{2}3\}<12\bar{2}3>$
Metals with $c/a \approx 1.623$ (Mg, Co)	Cod rolling	$\{0001\}<10\bar{1}0>$
Metals with $c/a > 1.623$ (Ti, Zr)	Cod rolling	$\sim\{11\bar{2}2\}<10\bar{1}0>$
$(\alpha_2+\beta)$ Ti$_3$Al	Hot rolling in near-α_2 phase field (~ 1123 K)	Mainly $\{0001\}<10\bar{1}0>$, with weak $\{1\bar{1}06\}[\bar{4}\bar{1}51]$ and $[\bar{4}403]$
AZ31 Mg Alloy	Hot extrusion plae (~ 570 K)	Mainly $\{0001\}$ basal fiber; with weak $\{10\bar{1}0\}$ and $\{11\bar{2}0\}$ fibers
AZ31 Mg Alloy	Recrystallization (~ 723 K) followed by hot extrusion	$\{0001\}$ basal and $\{10\bar{1}0\}$ fibers are retained, $\{11\bar{2}0\}$ fiber is strengthened
AZ31 Mg alloy	Secondary recrystallization (~ 800 K) followed by hot extrusion	$\{11\bar{2}0\}<10\bar{1}0>$
Ti-6A1-4V (α phase)	Hot rolling in α field (~ 1323 K)	$\{10\bar{1}0\}<11\bar{2}0>$
Ti40	Cold rolling	Strong $\{12\bar{2}3\}<10\bar{1}0>$ and weak $\{10\bar{1}3\}<11\bar{2}0>$
Ti40	Fully recrystallization (~ 973 K for 1 h)	$\{10\bar{1}3\}<11\bar{2}0>$

basal poles tilted away from the normal direction toward the transverse direction for Ti and Zr ($c/a < 1.633$). This is mainly contributed by the activation of different slip systems under different deformation modes. Also, the Texture strengthening and texture toughening in hexagonal materials have been observed in hexagonal metals, a similar effect as those observed in cubic materials.

The textures of cold-rolled hexagonal metals and alloys can be categorized into three groups according to their c/a ratios, namely materials with c/a ratios greater than, approximately equal to, and less than the ideal value of 1.633. Experimental results of the (0 0 0 2) pole figures for rolled Mg ($c/a = 1.624$), Zn (1.856) and Ti (1.588) are shown in Fig. 21.

In contrast to the well-established case for the FCC and BCC materials, the recrystallization texture in hexagonal material has been rarely studied. For HCP metals, rotations of $\sim 30°$ around [0001] and $\sim 90°$ around [10$\bar{1}$0] have been reported. The basal pole figures of recrystallized HCP metals are often essentially similar to those of rolling textures. The main basal texture components can be explained by the $\sim 30°$ rotation about [0001] makes orientation change between rolled and annealed textures. In fact, closer examination frequently reveals other types of textural change upon annealing. A very complete review on texture of hexagonal materials is due to Wang and Huang [62]. Table 4 shows various type

of textures observed in the processing of various HCP metals and alloys.

4.5. *Transformation texture*

Texture derived after transformation from high temperature phase depends upon the microstructural state of the parent phase. In many cases, the low-temperature behavior of these materials is derived from the processing done at elevated temperatures followed by phase transformations. The low temperature behaviour of these materials is sought from high temperature processes such as hot rolling hot forging etc. followed by phase transformations, both influencing the low temperature state of the materials. The improvements in product design for a given application require the formation of an adapted low temperature texture obtained from the texture of the high temperature state. This issue have been rigourously studied for the two important structural materials, namely (i) steels and (ii) titanium alloys and aluminides. During the hot rolling of steel, preceding the cold rolling process, the parent FCC austenite (γ) phase may develop a crystallographic texture, which is later inherited by the product BCC ferrite (α) after transformation. This inherited texture is also known as "transformation textures". The various kinds of transformation textures normally encountered in steels and the effects of compositional and processing variables on their development have been extensively reviewed by Ray and Jonas [54]. Similarly, the detailed account of these can be had in the comprehensive review by Ray and Jonas [55] as well in the paper by Suwas and Singh [63]. The effect of the crystallographic texture of high-temperature BCC phase on its transformation product, HCP, is largely documented for the many alloys, particularly for the alloy Ti-6Al-4V [64–66].

4.6. *The issue of strain path change: A new approach of texture tailoring*

A change in strain path during deformation processes is reported to change the plastic behaviour of metals to a large extent. Such changes are reported to affect texture formation. In fact, a change in strain path alters the substructure, which is developed as a result of prior course of deformation, and therefore affects the deformation texture. The change of the path of plastic deformation induces a destabilization of the substructure which is formed during the primary step of unidirectional rolling. A distinct change of texture is found depending on the deformation process. The change of the deformation path has a strong effect on the formation of texture. In particular, the texture stabilized during rolling becomes unstable and disintegrates when the rolling direction is changed from unidirectional to cross rolling. This results in unstable plastic flow of the material. This has been found to influence texture formation very significantly, an issue which was not adequately addressed earlier [67]. The author and his co-workers have carried out a series of investigation, that has shed some light in a few industrially important problems pertaining to strain path change. The study was carried out on FCC, BCC and HCP materials. Amongst FCC, copper and its alloys were studied thoroughly for processing – texture relationship [68–69], and its implication on formability [70]. A subsequent study on effect of modes of rolling and subsequent annealing on yield locus anisotropy and its dependence on microstructure and texture has revealed that the alloys exhibit marked anisotropy even after cross rolling. Annealing of the rolled materials brings down the extent of anisotropy [71]. The BCC alloy of titanium was also subjected to similar study, however, with a view to examine the effect of different texture on annealing and transformation behaviour of the material [72–73].

5. Texture evolution in intermetallics

Aluminide based intermetallic materials have been recognized as potential candidates for a variety of high-temperature structural applications capable of withstanding well beyond the operating temperatures of conventional materials. Because of their lower specific weights, remarkably high strength and improved oxidation resistance, the aluminide-based intermetallic compounds are still thought as the candidates for substituting the rather heavy superalloys atleast in some applications. At present their application is restricted in compressors and turbines of aircraft engines, however, investigations are being carried out to bridge the gap between their suitability for high temperature applications. Specifically designed thermomechanical processing schedule is generally used for forming these materials into suitable shapes for various applications. The processing route also influences the texture of the product, which in turn dictates the final properties [74–75]. Rigorous investigations have been carried out on processing-texture relationship in nickel, iron and titanium aluminides and included in two comprehensive reviews by Ray and Suwas [74–75].

The issue of texture is of extreme importance in these aluminides than the other two, by virtue of the fact that the processing as well as performance of HCP structured materials with regard to mechanical properties, is more sensitive to texture than a cubic material. Niobium modified titanium aluminides

based on Ti$_3$Al were viewed as potential candidates for bridging the gap between conventional titanium alloys and nickel base superalloys with regard to their temperature capabilities. The various thermomechanical processing routes have a pronounced effect on the development of textures in these materials, and therefore could influence the mechanical properties as well as anisotropy. It is well known that in order to achieve good ductility and formability in this alloy, a good basal texture is important in the rolled or rolled plus annealed materials. A comprehensive study of the texture developed/modifed was carried out to critically examine the evolution and stability of the hot/warm rolling texture as well as during subsequent heat treatments [76–80].

The yield locus was also determined for this alloy under different thermomechanically treated conditions in order to have an idea of mechanical anisotropy developed. It was found that a strong basal texture was responsible for yield locus anisotropy [81].

The final warm and cold rolling also affect the texture of the hot/warm rolled product. Moderate warm rolling of a prior thermomechanically processed alloy with a weak basal texture or a non basal texture did not either improve the basal texture or lead to the formation of basal texture. Moderate cold rolling of a prior thermomechanically processed alloy does not change its character although appreciable change in the microstructure is seen [82–83].

6. Texture in non metals
6.1. Ceramics
Texture in ceramics was studied in hard magnetic materials, high-temperature superconductors, ferroelectric, transformation-toughened ceramics and in surface layers of corrosive oxides. In general, the ceramic materials have lower crystal symmetries than metals and the anisotropy of many of their physical properties is much stronger. It is expected, therefore, that there will be also stronger influence of texture on the properties of ceramics than in highly symmetric metals. However, porosity and the presence of glassy phase influences the properties of these materials rendering the influence of texture of the crystalline part much smaller.

Ceramics are characterized by lower crystal symmetries (cubic to trigonal), higher lattice parameters, which result in a large number of diffraction peaks. This, in turn, leads to peak overlapping, especially at higher tilt angles in pole figure measurement. Hence the texture analysis in these materials requires additional peak separation techniques. The use of position sensitive detector combined with peak profile analysis programs is quite useful to determine the correct integrated intensity of overlapped and broadened peaks. The ODF computation also becomes complicated and requires a larger number of pole figures.

6.2. Evolution of texture in ceramics during processing
In ceramics, like metals, deformation and recrystallization leads to changes in texture. In addition to these, green compact or strip processing, stress-assisted densification and stress induced transformations, surface grinding, epitaxial growth etc may cause the formation of textures in ceramics. Processes like dry pressing, slip casting, pressure infiltration, tape casting {Fig. 22) and extrusion of monolithic ceramic materials with anisometric powder shapes give rise to the evolution of textures. Preparation of ceramic green bodies by slurry processing including slip casting, tape casting and pressure infiltration also give rise to textures in monolithic and composite ceramics. The most suitable approach to produce large volumes of sheet substrates with fairly uniform textures is tape casting, a processes involving slurry deformation consisting of primarily simple shear. Figure 22 shows texture change during tape casting process. The processes involving localised flow of the liquid carrier media, like slip casting and pressure infiltration can lead to very asymmetrical and inhomogeneous textures [84–85]. Wenk and Philips [86] have shown for an orthorhombic Bi-based superconductor that a strong basal texture can be produced in dry pressed materials with a platy grains. The material has highly anisotropic surface characteristics, which, through repeated heat treatment and grinding cycles, led to mica-like grain shapes with [001] normal to the long grain surfaces.

Application of centrifuging to slurries is another way to produce textured ceramics prior to firing. Centrifugal casing and centrifugal slip casting processes result in strongly textured ceramic. In sintered centrifuged ceramic composite slurry containing alumina platelets, fine alumina powder and fine zirconia powder, the strong texture of the alumina platelets is intensified during grain growth since the large alumina platelets grow at the expense of finer alumina grains. Centrifugal slip casting processes is a viable process for the production of tube shaped ceramic components. When this process is employed on materials with anisometric grain shapes, this may result in strong texture in the material. Extrusion processes in the presence of plastic binders which are burnt out prior to high temperature consolidation via sintering lead to the development of textures. The combination of

Figure 22: Texture evolution in ceramic processing by tape casting [Courtesy: H.-J. Bunge, Texture and Microstructure].
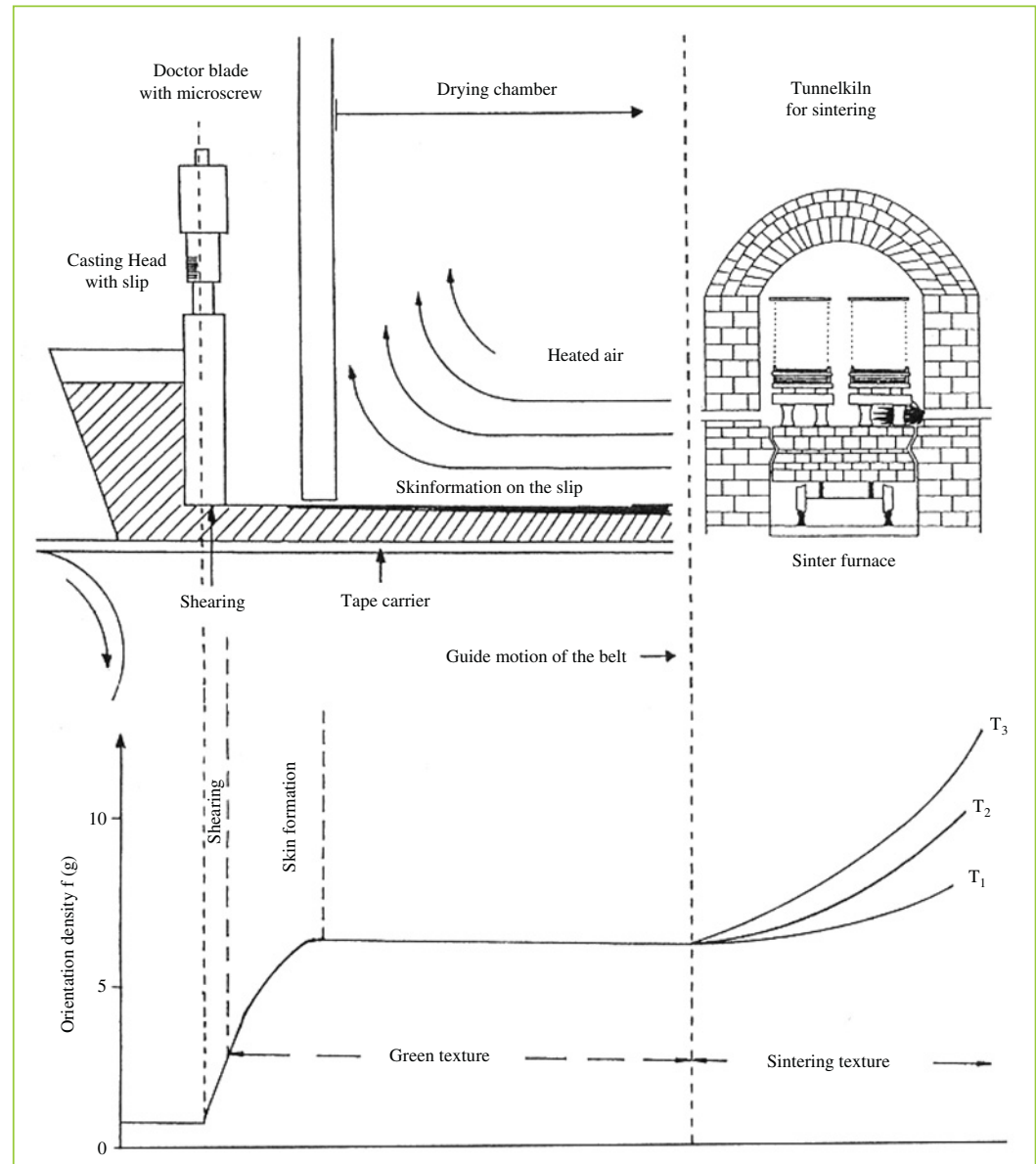
directional processing and anisometric grain shapes lead to fairly simple textures.

Processes like hot-pressing, hot forging, extrusion and plane strain compression commonly employed in ceramic processing and forming, lead to the development of textures in an initially random ceramic material. The mechanisms leading to texture formation in these cases are, apart from rotation of anisometric grains, the dislocation slip, recrystallisation, twinning and growth of oriented grains. The most extensive study of texture development in the structural ceramics have been

carried out on Alumina [87–88], Silicon Nitride [89–91] and a number of ceramic composites [92–93].

6.3. *Polymers*

The bonding nature in polymers imparts a strong anisotropy to properties in the crystalline polymers. Consequently, texture plays an even more important role in controlling properties in polymers. The pole figure analysis in such materials is carried out by wide-angle X-ray diffraction. Various studies [94–98] on texture evolution during deformation by uniaxial tension and compression, bi-axial tension

and shear suggests that different mechanisms of deformation are prevalent in polymers at different ranges of imposed strain for any particular mode of deformation. Relaxation is an inherent mechanism of deformation in polymers. As soon as the load is taken off the sample in the deformation experiments, relaxation processes initiate automatically. These can produce large unloading strains, especially in tensile loaded samples, and potentially cause significant changes in the underlying texture in the sample. Textures reported in these studies [99–108] correspond to "deformed and relaxed" textures in the samples.

Recently the paper due to Li et al. [109] provides several new insights into texture development in tensile straining of a polymer, high-density polyethylene, to large strains. At least three distinct preferred orientations were detected, namely (i) a component with (001) plane aligned along the extension axis, (ii) a component with the plane (011) aligned close to the extension axis, and (iii) a component with plane (010) aligned along the extension axis. Note that only the first component has been reported to be stable at high strains in previous studies. The natural relaxation of strain following the tensile loading had a significant impact on the texture in the sample. It was observed that the relaxation process mitigated or eliminated the second and third preferred texture components described above, while strengthening the first.

6.4. *Texture in thin films, coating and interconnect*

All most all deposited films and coatings possess some texture depending on material and experimental parameters. The difference between texture of bulk materials and that of films is that films often exhibit a one-degree orientation in such a way that every crystallite has tendency to possess a definite crystallographic axis along the deposition direction. Texture evolution in thin films and coatings is probably as well known as their bulk counterparts. The first available reference is due to Volmer [110], who reported that zinc crystals grown from a vapour beam had a preferred orientation with respect to the vapour beam direction. Till date several investigations have been carried out in vapour deposited films as well as films prepared by other techniques, for example, films electrodeposited from aqueous solutions.

The oxidation rates of polycrystalline Ni and Ti depend on crystallographic texture and surface finish. For high-purity Ni, oxidized at temperature below 1023°C, the differences in oxide growth on differently oriented crystal faces reach up to one order of magnitude. These differences are caused by

the microstructure of oxide and in particular grain size and grain boundary structure. Modification of substrate texture can be an effective way to improve oxidation resistance of metals and alloys.

The properties of electrolytic coatings depend on their crystallographic texture. The texture of coatings can be modified by electrodeposition conditions. Since oxidation is a surface phenomenon, the improvement in oxidation resistance may be obtained by modifying the texture of the surface layer of material. In case of Ni and its alloys, the increase in strength of (111) component results in a significant increase in the oxidation resistance [111–112].

The directional dependence of the dielectric constant may depend on the arrangement of the polymer chains/crystallites in the film so a detailed understanding of microstructure and texture of polymer thin film is important. X-ray pole figure technique has been effectively used to quantify the texture of parylene films on a Si substrate and is interpreted to determine parylene molecular orientations within the crystallites along with the distributions of the oriented polymer crystallites [113]. The texture of vapor deposited parylene thin films on Si has been successfully measured using X-ray pole figure technique to quantify the crystalline portion.

The performance of deposited metal films in electronic interconnect structures is a sensitive function of texture. For example, Al-based interconnects with a large uniform grain size and a strong <111> texture provide significantly improved reliability [114]. It is, therefore, necessary to have a proper understanding of processing-texture relationship in interconnects for the development and design of reliable interconnects structures. The microstructural evolution of polycrystalline films during deposition and annealing occurs by recrystallization or the competitive growth of grains via the motion of grain boundaries. The driving forces for grain boundary motion include curvature of the grain boundary, surface and interfacial energy differences between competing grains, and strain energy differences between adjacent grains. The crystallographic orientation of grains helps to determine the magnitude of surface and interfacial energies as well as the magnitude of strain energy.

The textures of polycrystalline vapor-deposits [115–117], electro-deposits [117–123] and electroless-deposits [124–125] depend on process variables. When annealed, the deposits may undergo texture changes. The texture turnover is controlled by grain growth or recrystallization, depending on the dislocation density in the deposits. When the

dislocation density is very high, the directionality of the stress field caused by the dislocations dominates the recrystallization texture [117–120]. When the dislocation density is low, as in deposits whose grain sizes are of the order of 10 nm or less, the annealing texture is controlled by interface energy, grain boundary energy and mobility, surface energy, and strain energy [117]. In this case, already existing grains that have lower interface, grain boundary, surface, and strain energies and higher grain boundary mobility are in a better position to grow and dominate the texture. This growth texture does not need nucleation for the evolution of texture. Most Cu and Al deposits in interconnects are known to have the <111> texture, in which the {111} planes are normal to the film growth direction. The sputtered Al deposits are very thin, and their textures are determined by the minimization of interface and surface energies, which gives rise to the <111> texture. Damascene-processed Cu deposits are usually obtained by sputtering, followed by electrodeposition. The sputter-deposited Cu layer is usually about 100-nm thick and has the <111> texture, which is inherited by the subsequent Cu electrodeposit up to a critical thickness. Above the critical thickness, the texture changes if electrolysis conditions differ from those that give rise to the <111> texture.

7. Texture development in ultrafine grain and nanostructured materials

Almost since past one decade, tailoring microstructure with ultrafine grain sizes in bulk materials has triggered a lot of interest amongst the scientific community. A number of innovative, non-conventional processes of fabrication have been proposed and experimented, namely high pressure torsion, multi-axial forging, accumulative roll bonding and equal channel angular extrusion. Of all these techniques, equal channel angular extrusion (ECAE), is the most widely investigated technique and has been successfully applied to materials with different crystal structures [126–132]. Equal channel angular extrusion (ECAE) is being viewed as one of the potential deformation processing techniques for grain refinement to submicron size or sometimes up to nano-meter size of bulk materials. The process is also associated with the development of specific crystallographic textures, which add to the mechanical characteristics of the as-processed materials. In ECAE, a billet of circular or square cross section is deformed in a narrow deformation zone at the plane of intersection of two die channels of the same cross section and the strain mode approximates closely to simple shear. As the overall billet geometry remains nearly constant during

ECAE, multiple passes through the die are possible without any reduction in cross-sectional area. This allows materials to be deformed to very high plastic strains (per pass) that cannot be readily obtained in more conventional processes, such as rolling.

In this deformation process, it is assumed that texture developed and its relationship with the shear plane are the key factors that affect grain refinement in subsequent stages. The author of this review along with co-workers has carried out an extensive work in this area on FCC, HCP as well as BCC materials. Amongst the FCC metals, aluminium [133–134] and aluminium alloys [135–136], copper [136–140] and silver [141–143], were studied and a clear effect of deformation variables like strain and strain path [133] as well as material variables like purity [133, 137], alloying addition [144] , initial microstructure and texture [139, 145], stacking fault energy [146–147] has been documented. Although in such situations it was difficult to clearly isolate the individual effects of each of the preceding variables on texture evolution, it was worth examining the conditions in order to know the limits that could be implemented from the view point of texture engineering. The textures obtained by this process are associated with gradient, which has been further investigated in detail by synchrotron X-ray texture measurement [138, 142]. Further response of recrystallization annealing was also studied for copper [148].

The HCP materials are found even more sensitive to process variables implemented during ECAE [149–150]. An additional attribute of texture in ECAE was its clear role in imparting workability in magnesium, which had otherwise very poor ductility. Since these materials are processed at higher temperatures, associated dynamic recrystallization was also studied from the view point of texture development [151].

8. Texture in Geology and Geophysics

In geology, texture investigations are applied because of three reasons: (i) to deconvolute the deformation history of rocks, e.g. to determine the direction of tectonic transport from the symmetry of the mineral textures, (ii) to model anisotropic physical rock properties, e.g. the propagation velocity of elastic waves in order to obtain information about the seismic behaviour of the earth's interior, and (iii) to discover the mechanisms of texture formation. Texture of deep ice cores at places like Greenland and Vostok has been studied in an attempt to reconstruct the past climate as well as atmospheric composition by Castelnau [152]. Wenk [153] has also studied the transformation and deformation behaviour of another polymorph of ice (ice II) to

Figure 23: Bar graph showing the record of publications related to texture for the last 25 years as obtained from ISI Web of Knowledge.
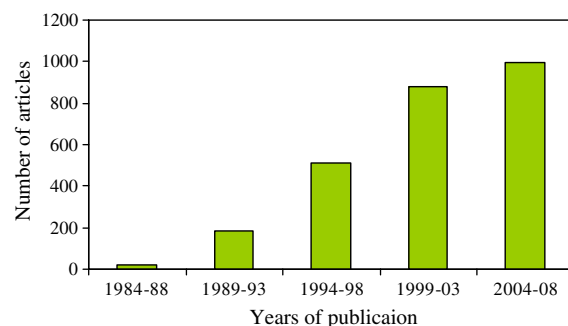
understand the deformation mechanisms operative during flow. Mineralized biological materials like mollusc shells, skeletons, bones and teeth show a wide variety of textures. The measurement of texture of these materials has become possible due to advancement in X-ray and neutron diffraction facilities and researchers have made an attempt to study the effect of texture on hydroxyapatite bone implants [154–155].

9. Summary and perspectives

The presence of texture in crystalline materials is not an exception but a rule. Anything and everything that is crystalline has some texture either weak or strong and it is a challenge to prepare a completely random polycrystalline material. Our understanding of texture has been greatly facilitated by (i) the advent of sophisticated instrumentation like the texture goniometer with high precision detectors, (ii) Bunge's pioneering work in developing the concept of orientation distribution function, (iii) development of Electron Backscattered Diffraction (EBSD) and the recent advancement in performing in situ X-ray, neutron and Synchrotron radiation based experiments to name a few.

In the present review, an attempt has been made to summarise the importance of texture in a variety of materials ranging from rocks and bones, shells and ice to normal metals and alloys, polymers and ceramics and various functional materials like thin films and interconnects. It is now developed into a multidisciplinary field that spans various domains of science like metallurgy, ceramics, polymers, semiconductor physics, geology and biology. The advancement in the characterization facilities has made it possible to expand the domain of texture studies from geophysics to device physics. Also, a deeper insight into various deformation and

transformation mechanisms in conventional metals and alloys can be obtained using in situ neutron and synchrotron diffraction facilities developed around the world.

The scope of texture research has been increasing at a rapid pace and this is manifested by a sharp increase in the number of publications over the years (Fig. 23). It is to be mentioned here that the number of journals wherein articles on texture have been published has also increased indicating the inroads texture investigation has made into fields like biomaterials and thin films. The advent of better characterization facilities have helped to address many long standing issues in texture, at the same time have opened many issues. Without being prophetical, the authors would like to conclude that these problems will keep the coming generation of texture researchers busy.

Acknowledgements

References
1. Heatherly M. and Hutchinson W. B., *An Introduction to Texture in Metals*, Monograph no. 5, The Institution of Metallurgist London 1979.
2. Bunge H. J., *European J. of Mineralogy*, 9 (1997) 735.
3. Barrett C. S. and Massalski T. B., *Structure of Metals*, McGraw Hill, NewYork, 1966.
4. Cullity B. D., *Elements of X-ray Diffraction*, Addison-Wesley, 1978.
5. Roe R.-J, *Journal of Applied Physics* 36, (1965) 2024.
6. Bunge H. J., *Z. Metallk.* 56 (1965) 872.
7. Schulz L. G., *J. Appl. Phys.*, 20 (1949 a and b) 1030.
8. Cahn R. W., *Materials Science and Technology*, Volume 15, Processing of Metals and Alloys, Wiley, 1991.

9. Kocks U. F., Tome C. N. and Wenk H. R., *Texture and Anisotropy*, Cambridge University Press, 1998.

10. Bunge H. J., *Texture Analysis in Materials Science - Mathematical Methods*, Buttersworth London. 1982.

11. Lucke K. and Pospeich J., *Texture Analysis of Cubic Crystals*, Springer Verlage, Berlin 1988.

12. Matthies S. and Vinel G. W., *Phys. Stat. Sol.* (b)112 (1982) K111.

13. Pawlik K., Pospiech J, Lucke K., *Textures Microstruct.*, 14–18 (1991) 25.

14. Dingley D. J., *Scanning Electron Microscopy* 4 (1981) 273.

15. Dingley D. J. and Randle V., *J. Mater. Sci.*, 25 (1992) 4545.

16. Brockhouse B. N., Canad. *J. Phys.* 31 (1953) 339.

17. Bacon G. E., *Neutron Diffraction*, Oxford: Clarendon Press. 1975.

18. Guiner A and Graf R., *Acta Crystallogr.* 5 (1952) 150.

19. Wever F., *Z. Phys.*, 28 (1924) 69.

20. Bunge H. J. and Klein H., *Z. fur Metallk.* (Germany) 87 (1936) 465.

21. Bruckner G., Reher F. R. And Gottstein G., *Textures and Microstructures* 30 (1998) 125.

22. Randle V. and Engler O., *Introduction to Texture Analysis Macrotexture, Microtexture and Orientation Mapping*, Gordon and Breach Science Publishers, 2000.

23. Schwarzer R.A. and Weiland H., *Textures Microstruct.*, 8–9 (1988) 443.

24. Schwarzer R. *Z., Metallkd.* 85:88 (1994) 585.

25. Wright S. I.. and Dingley D. *J., Proc. EUROMAT* 4 (1999) 253.

26. S. Zaefferer, *J. Appl. Cryst.* 33 (2000) 10.

27. Otte H. M., Dash J.and Schaake H. F., *Phys. Stat. Sol.* 5 (1964) 527.

28. Schwarzer R. A., *Ultramicroscopy* 67 (1997) 19.

29. Sztwiertnia K. and Haessner F., *Mater. Sci. Forum* 157–162 (1994) 1069.

30. Fundenberger J. J., Morawiec A., Bouzy E. and Lecomte J. S., *Ultramicroscopy* 96 (2003) 127.

31. Sayers C. M., Allen D. R. Haines G. E., Proudfoot G., Wadley H. N. G., Thompson R. B. and Almond E, *Phil. Trans. R. Soc. Lond*. A 320 (1986) 187.

32. Schmid E. and Boas E., *Plasticity of Crystals*, Hughes Co., London 1950.

33. Taylor G. I., *J. Inst. Met.*, 62 (1938 a and b) 307.

34. von Mises R., *Z. fur Angewandte Mathematik and Mechanik*, 8 (1928) 161.

36. Bishop J. F. W. And Hill R., *Phil. Mag.* 42 (1951a) 414.

36. Bishop J. F. W. And Hill R., *Phil. Mag.* 42 (1951b) 1298.

37. Fleischer R. L., *Acta Metall.*, 35 (1987) 2136.

38. Doherty R. D., Gottstein G., Hirsch J., Hutchinson W. B., Liicke K., Ned E. and Wilbrandt P.J., *Proc. ICOTOM* 8 (1988).

39. Doherty RD, Kashyap K, Panchanadeeswaran S. *Acta Metall Mater.*, 41 (1993) 3029.

40. Doherty RD. *Prog Mater Sci* 42 (1997) 39.

41. Humphreys F. J. and Hatherly M., *Recrystallization and related annealing phenomena,*. London: Pergamon Press (2002).

42. Weiland H. In: Hansen N, Jensen DJ, Liu YL, Ralph B, editors. *Proceedings of the 16th Riso international symposium on materials science: microstructural and crystallographic aspects of recrystallization*, (1995) 215.

43. Samajdar I. and Doherty R. D., *Acta Mater* 46 (1998) 3145.

44. Jensen D. J., Larsen A. W., *Mater. Charact.* 51 (2003) 271.

45. Hutchinson, W. B., *Metals Rev.*, 29 (1984) 25.

46. Taheri M. L., Molodov D., Gottstein G. and Rollett A. D., *Z. Metall.* 96 (2005) 1166.

47. English A. T. and Chin G. Y., *Acta Metall.*, 13 (1965) 1013.

48. Lucke K., *Proc. Sixth Int. Conf. Text. Mater.* 1(1981) 14.

49. Ray R. K., *Acta. Metall. Mater.*, 43 (1995) 3861.

50. Makita H., Hanada S. and Izumi O., Acta Metall. 36 (1988) 403

51. Doherty R. D., Hughes D. A., Humphreys F. J., Jonas J. J., Juul Jensen D., Kassner M. E., King W. E., McNelley T. R., McQueen H. J., Rollett A. D., *Materials Science and Engineering A*, 238 (1997) 219.

52. Doherty R. D., *Prog. In Mat. Sci.*, 42 (1997) 39.

53. Suzuki T., Arai K., Shiga M. And Nakamura Y., *Metall. Mater. Trans.* 16 A (1985) 27.

54. Ray R. K. and Jonas J. J., *Int. Mater. Reviews*, 35 (1990) 1.

55. Ray R. K., Jonas J. J. and Hook R. E., *Int. Mater. Reviews*, 39 (1993) 129.

56. Ray R. K., Jonas J. J., et al., *ISIJ International*, 12 (1994) 927.

57. Charles O.S., *Nuclear reactor materials*. In: Addison-Wesley, Reading, MA 1967.

58. Maussner G., Ortlieb E. and Weidinger H.-G., *Materials for nuclear reactor core applications,*, BNES, London 1987.

59. Hanson B. H., *Mater. Des.* 7 (1986) 301.

60. Leyens C. and Peters M., *Titanium and Titanium Alloys: Fundamentals and Applications*, Wiley-VCH 2003.

61. Conard H., *Prog. Mater. Sci.*, 26 (1981) 123.

62. Wang Y. N. and Huang J. C., *Materials Chemistry and Physics*, 81 (2003) 11.

63. Suwas S, Singh A. K., *Metall. and Mater. Trans.* 35 A (2004) 925.

64. Dey S. R., Germain L. and Humbert M., *Phil. Mag. Letters*, 85 (2005) 463.

65. Suwas S. and Ray R. K., *Mater. Sci. Engg.* 391 A (2005) 249.

66. Dey S. R., Suwas S., Fundenberger J.J., et al. *Mater. Sci. Engg.* 483 A (2008) 551.

67. Bocker A. and H. J. Bunge, Textures and Microstructures, 14–18 (1991) 1037.

68. Suwas S, Singh A. K., Rao K. N., et al., *Z. fur Metallk.* 93 (2002) 918.

69. Suwas S., Singh A. K., Rao K. N., et al., *Z. fur Metallk.* 93 (2002) 928.

70. Suwas S, Singh A. K., *Mater. Sci. Engg.* 356 A (2003) 368.

71. Suwas S, Singh A. K., Rao K. N., et al. *Z. fur Metallk.* 94 (2003) 1313.

72. Gurao N. P., Ali Ashkar Ali A and Satyam Suwas, *Mat. Sci. Engg.* A. (submitted)

73. Suwas Satyam, Gurao N. P. and Ashkar Ali A, *ICOTOM 15* 2008.

74. Suwas S, Ray R. K., *Metall. And Mater. Trans.,* 31 A (2000) 2339.

75. Ray R. K., Suwas S., *Metals and Mater. Int.*, 6 (2000) 39.

76. Suwas S, Ray R. K., *Scripta Mater.* 44 (2001) 275.

77. Suwas S, Ray R. K., Singh A. K., et al., *Acta Mater.*, 47 (1999) 4585.

78. Suwas S. and Ray R. K., *Acta Mater.*, 47 (1999) 4599.

79. Suwas S. and Ray R. K., *Bulletin of Mater. Sci.*, 22 (1999) 581.

80. Ray R. K. and Suwas S., *Metals Materials and Processes*, 10 (1998) 265.

81. Suwas S., Lahiri I., Ray R. K., et al., *Mater. Letters* 57 (2003) 3251.

82. Suwas S., Singh A. K., Ray R. K., et al., *Scripta Mater.* 35 (1996) 897.

83. Suwas S. and Singh A. K., *Mater. Sci. Engg.* A 356 (2003) 368.

84. Bocker A, Brokmeier H. G. and Bunge H. J., *J. Eur. Ceram. Soc.*, 7 (1991) 187.

85. Dimarcello F. I., Key F. L., *J. Amer. Ceram. Soc* 55 (1972) 509.

86. Wenk H. R. and Phillips D., *Physica C* 200 (1992), 105.

87. Ma Y., Bowman K. J., *J. Amer. Ceram. Soc.*, 74 (19991) 2941.

88. Lee C. S., Duggan B. J. and Smallman R. E., *Phil. Mag. Lett.* 68 (1993) 185.

89. Wilkens C.A., Corbin N. D., et al., *Ceram. Eng. Sci. Proc.*, 9 (1988) 1367.

90. Lee F. and Bowman K. J., *J. Amer. Ceram. Soc.*, 75 (1992) 1748.

91. Lee F. and Bowman K. J., *J. Amer. Ceram. Soc.*, 77 (1994) 947.

92. Sandlin M. S. and Bowman K. J., *Ceram. Eng. Sci. Proc.*, 13 (1992) 661.

93. Lee F., Sandlin M. S. and Bowman K. J., *J. Amer. Ceram. Soc.*, 76 (1993) 1793.

94. Butler M. F., Donald A. M. and Ryan A. J., *Polymer* 39 (1998) 39.

95. Butler M. F.,. Donald A. M. and Ryan A. J.. *Polymer* 39 (1998) 781.

96. Butler M. F. and Donald A. M., *Macromolecules* 31 (1998) 6234.

97. Butler M. F., Donald A. M., Bras W. and Mant G. R., *Macromolecules* 28 (1995) 6383.

98. Hiss R., Hobeika S., Lynn C. and Strobl G., *Macromolecules* 32 (1999) 4390.

99. Bartczak Z., Galeski A., Argon A. S. and Cohen R. E., *Polymer* 37 (1996) 2113.

100. Bartczak Z., Cohen R. E. and Argon A. S., *Macromolecules* 25 (1992) 4692.

101. Bartczak Z., Argon A. S. and Cohen R. E., *Macromolecules* 25 (1992) 5036.

102. Lee B. J., Argon A. S., Parks D. M., Ahzi S. and Bartczak Z., *Polymer* 34 (1993) 3555.

103. Pazur R. J., Ajji A. and Prud'homme R. E., *Polymer* 34 (1993) 4004.

104. Krause S. J. and Hosford W. F., *J Polym Sci. Polym Phys Ed* B27 (1989) 1853.

105. Song H. H., Argon A. S. and Cohen R. E., *Macromolecules* 23 (1990) 870.

106. Young R. J. and Bowden P. B., *Philosophical Mag.* 29 (1974), 1061.

107. Pazur R. J. and Prud'homme R. E., *Polym.Sci Polym Phys Ed* B32 (1994), 1475.

108. Bartczak Z., Argon A. S. and Cohen R. E., *Polymer* 35 (1994), 3427.

109. Li D., Garmestani H., Kalidindi S., and Alamo R., *Polymer* 42 (2001) 4903.

110. Volmer M., Z. Phys. 5 (1921) 31.

111. Czerwinski F., Zhilyaev A., Szpunar J. A., *Corrosion Science* (1999) 1703.

112. Czerwinski F., Szpunar J.A., *Mater. Sci. Forum* 204-206 (1996) 49.

113. Stutzman N. S., Smits E., et al., *Nature Materials*, 4 (2005) 1.

114. Lee D. N. and H. J. Lee, Journal of Electronic Materials, 32 (2003) 1012.

115. Lee D. N, *J. Mater. Sci.* 24, (1989) 4375.

116. Lee D. N., *J. Mater. Sci.* 34, (1999) 2575.

117. Lee D. N., *Mater. Sci. Forum* 75, (2002) 408.

118. Lee D. N., S. Kang, and J. Yang, *Plat. Surf. Finish.*, 5(1995) 76.

119. Lee D. N., *MRS Symp. Proc.* 427 (1995) 168

120. Choi J.-H and Lee D. N., *J. Mater. Sci.* 35, (2000) 4055.

121. Ye G.C. and Lee D. N., *Plat. Surf. Finish.* 68, (1981) 60.

122. Lee D. N. and Ye G. C., *Plat. Surf. Finish.* 68, (1981) 46.

123. Nam H-S and Lee D. N., *J. Electrochem. Soc.* 146 (1999) 3300.

124. Hur K.-H., Jeong J.-H, and Lee D. N., *J. Mater. Sci.* 25 (1990) 2573.

125. Hur K.-H, Jeong J.-H, and Lee D.N., *J. Mater. Sci.* 26 (1991) 2037.

126. Valiev R. Z., Islamgaliev R. K., Alexandrov I. V., *Prog Mat. Sci.*, 45 (2000) 103.

127. Wetscher F., Vorhauer A., Stock R. and Pippan R., *Mater Sci. Eng. A*, 387 (1999) 809.

128. Vorhauer A. and R. Pippan, *Scripta Mater* 51 (2004) 921.

129. Balakrishna Cherukuri, Teodora S. Nedkova and Raghavan Srinivasan, *Mater Sci. Eng. A*, 410 (2005) 394.

130. Baojun Han, Zhou Xu, *Mater. Sci. Eng* A, 447 (2007)119.

131. Tsuji N., Saito Y., Utsunomiya H. and Tanigawa S., *Scripta Mater.*, 40 (1999), 795.

132. Saito Y., Utsunomiya H., Tsuji N. and Sakai T., *Acta Mater*, 47 (1999) 579.

133. Suwas S, Toth L. S., Fundenberger J. J., et al., *Texture and Anisotropy of Polycrystals II*, 105 (2005) 357.

134. Skrotzki W., Scheerbaum N., Oertel C. G., et al., *Acta Mater.*, 55 (2007) 2211.

135. Skrotzki W., Scheerbaum N., Oertel C. G., et al., *Texture and Anisotropy of Polycrystals II*, 105 (2005) 351.

136. Skrotzki W., Scheerbaum N., Oertel C. G., et al., *Nanomaterials By Severe Plastic Deformation*, 503–504 (2006) 99.

137. Toth L. S., Massion R. A., Germain L., et al., *Acta Mater.,* 52 (2004) 1885.

138. Skrotzki W., Scheerbaum N., Oertel C. G., et al., *Texture and Anisotropy of Polycrystals II,* 105 (2005) 327.

139. Suwas S, Arruffat-Massion R, Toth L. S., et al., *Metall. And Mater. Trans.,* 37 A (2006) 739.

140. Skrotzki W., Scheerbaum N., Oertel C. G., et al., *Acta Mater.,* 55 (2007) 2013.

141. Suwas S., Toth L. S., Fundenberger J. J., et al., *Scripta Mater.,* 49 (2003) 1203.

142. Skrotzki W., Scheerbaum N., Oertel C. G., et al. *ICOTOM 14, Textures of Materials Parts I and II,* 495–497 (2005) 821.

143. Beyerlein I. J., Toth L. S., Tome C. N., et al., *Philosphical Magazine,* 87 (2007) 885.

144. Suwas S., Biswas S., et al., *Material Science Forum*, 584–586 (2008) 585.

145. Goran D., Fundenberger J. J., Suwas S, et al., *ICOTOM 14, Textures of Materials Parts I and II,* 495–497 (2005) 333.

146. Suwas S, Toth L. S., Fundenberger J. J., et al., *Texture and Anisotropy of Polycrystals II,* 105 (2005) 345.

147. Arruffat-Masion R, Suwas S., Toth L. S., et al., *ICOTOM 14, Textures of Materials Parts I and II,* 495–497 (2005) 839.

148. Suwas S. and Dong IkKim, *Material Science Forum*, 558–559 (2007) 1353.

149. Beausir B., Suwas S., , et al. *Acta Mater.,* 56 (2008) 200.

150. Suwas S., Gottstein G. and Kumar R., *Mater. Sci. Engg.* 471 A (2007) 1.

151. Beausir B., Suwas S., Toth L. S., et al., *ICOTOM 15* 2008.

152. Castelnau O., Shoji H., et al., *u* 154 (1998) 307.

153. Bennett K., Wenk H. R., Durham W. B, Stem L. A. and Kirby S. H., *Phil. Mag.*, 76 A (1997) 413.

154. Benmarouane A., Hansen T. and Lodini A., *Physica B*, 350, (2004) E573.

155. Benmarouane A., Citterio-Bigot H., et al., *Material Science Forum,* 571–572 (2008) 163.

Satyam Suwas is Assistant Professor in the Department of Materials Engineering at Indian Institute of Science Bangalore. He obtained his Ph.D. from Indian Institute of Technology, Kanpur. Prior to joining I.I.Sc., he worked briefly at Defence Metallurgical Research Laboratory, Hyderabad as a Scientist, at University of Metz France as visiting Assistant Professor and at RWTH, Aachen, Germany as Alexandar von Humboldt fellow. His current research interests are crystallographic texture evolution and grain boundary engineering in structural and functional materials, ultra-fine and nano-structured materials and high temperature materials. He has published over 60 papers in international journals and conferences.

Nilesh Prakash Gurao is doctoral student in the field of "Deformation texture evolution in close packed materials" in the Department of Materials Engineering at the Indian Institute of Science, Bangalore. He had received his Bachelor of Engineering (B.E.) degree in Metallurgical and Materials Engineering from Visvesvaraya National Institute of Technology (VNIT), Nagpur, Maharashtra, India in May 2005. He worked for TATA MOTORS, Pune for a brief stint before moving to I.I.Sc. for his doctoral degree.